Bangor University

DOCTOR OF PHILOSOPHY

Optimal operating conditions and security considerations for optical chaos communications

Priyadarshi, Sanjay

Award date:
2013

Awarding institution:
Bangor University

DOCTOR OF PHILOSOPHY

Optimal operating conditions and security considerations for optical chaos communications

Priyadarshi, Sanjay

Award date:
2013

Optimal Operating Conditions and Security Considerations for Optical Chaos Communications

Submitted by Sanjay Priyadarshi

for the degree of

Doctor of Philosophy

Bangor University

2013

To My Parents and Namrata

Acknowledgements

I would like to express my hearty gratitude to my supervisor Prof. K Alan Shore for his guidance and support; thank you Prof. Alan. Without his tirelessly effort, this thesis would not have been completed. I would like to thank Bangor University 125th Anniversary Research Scholarship for financially supporting this work. I would like to thank Prof. Paul S. Spencer for financial support after the end of anniversary scholarship. I would like to thank Dr. Iestyn Pierce for helping in Matlab and Fortran programming and continuous encouragement and motivation. I would like to thank Dr. Yanhua Hong for her guidance, comments and helping in lab experiments. I would also like to thank Nada Rawi for help with the experiments.

Last, but not least I thank my parents, wife, family and friends for their moral support and encouragements from time to time.

Abstract

This thesis details research on chaos-based optical communications using semiconductor lasers. Theoretical work has identified optimal operating condition of optical chaos communications systems without the need for re-adjustment of laser operating conditions in the field. In addition, an experimental investigation has been undertaken of one aspect of the security of message transmission using chaotic semiconductor lasers and specifically using Vertical-Cavity Surface-Emitting Laser (VCSEL).

In optical chaos communications a message is masked in the noise-like broadband output of a chaotic transmitter laser, and message recovery is enabled through the synchronization of the transmitter and the (chaotic) receiver laser. Key issues are to identify the laser operating conditions which provide the highest quality synchronization conditions and those which provide optimized message extraction. In general such operating conditions are not coincident.

In this thesis numerical simulations are performed with the aim of identifying a regime of operation where the highest quality synchronization and optimizing message extraction efficiency are achieved simultaneously for the analogue and digital message modulation. Use of such an operating regime will facilitate practical deployment of optical chaos communications systems without the need for re-adjustment of laser operating conditions in the field.

In this way it has been found, for example, that in an optical chaos communication system an optimal configuration for 1 GHz modulation frequency may utilize a 2% modulation depth and 20% coupling rate from transmitter laser to receiver laser for analogue message modulation.

Ideal operating conditions for digital message modulation, identified using the laser bias current as the control parameter, are found for 2GB/s message transmission and a modulation depth of about 2%.

An experimental study has also been undertaken to determine the effect of time delay and concealment in the external cavity semiconductor laser systems. The time delay (TD) signature arises due to the external cavity round trip time of feedback in the external cavity semiconductor laser system. The identification of the time delay may affect the security of encoded messages.

An external cavity VCSEL with variable optical-polarization-angle feedback has been explored experimentally in order to identify conditions for time delay concealment.

In this work the VCSEL was subject not only to variable optical polarization angle of feedback but also variable optical feedback strength and bias current. The TD signature concealment is evaluated through the use of an autocorrelation function and an information theory-based permutation entropy function. It was found that the TD signature is concealed at low feedback strength of order –18 dB. At moderate feedback strengths, the TD signature is sensitive to the rotation of the polarization angle of the optical feedback with TD concealment being observed for polarization angles in the range from 45° to 90°.

Publications

Journal Papers

S. Priyadarshi, Y. Hong, I. Pierce and K. Alan Shore, "Experimental Investigations of Time-Delay Signature Concealment in Chaotic External Cavity VCSELs Subject to Variable Optical Polarization Angle of Feedback", IEEE Journal of Selected Topics in Quantum Electronics, vol. 19, no. 4, pp. 1700707, July/August 2013.

S. Priyadarshi, I. Pierce, Y. Hong and K. Alan Shore, "Optimal operating conditions for external cavity semiconductor laser optical chaos communication system", IOP Semicond. Sci. Technol. Vol. 27, issue 9, pp. 094002, Aug. 2012.

Yanhua Hong, Cristina Masoller, Maria S. Torre, Sanjay Priyadarshi, Abdulqader A. Qader, Paul S. Spencer, and K. Alan Shore, "Thermal effects and dynamical hysteresis in the turn-on and turn-off of vertical-cavity surface-emitting lasers", Opt. Lett. vol. 35, pp. 3688, Nov. 2010.

Conference Papers

S. Priyadarshi, Y. Hong, I. Pierce and K. A. Shore, "Optimal Operating Regime for Digital Optical Chaos Communications", Proceeding of European Optical Society Annual Meeting 2012 Aberdeen Scotland, UK, 25th – 28th September 2012.

S. Priyadarshi, I. Pierce, Y. Hong and K. A. Shore, "Optimal Operating Conditions for Optical Chaos Communication Systems Using External Cavity Semiconductor Lasers", Proceeding of semiconductor and integrated optoelectronics Cardiff, UK, 2nd -4th April 2012.

S. Priyadarshi, I. Pierce, Y. Hong and K. A. Shore, "Message Extraction in Diode Laser Based Optical Chaos Communications, Proceeding of semiconductor and integrated optoelectronics Cardiff, UK, 18th-20th April 2011.

List of Acronyms

ACF	Auto-Correlation Function
BER	Bit Error Rate
BRBS	Binary Random Bit Sequence
CPF	Chaos Pass Filtering
DFT	Discrete Fourier Transform
DTFT	Discrete-Time Fourier Transform
DTR	Data Transmission rate
FFT	Fast Fourier Transform
MDC-SL	Mutually Delay-Coupled Semiconductor Laser
OA	Optical Attenuator
PE	Permutation Entropy
PSMR	Peak Signal to Mean Ratio
QWP	Quarter Wave Plate
RL	Receiver Laser
ROF	Relaxation Oscillation Frequency
SNR	Signal to Noise Ratio
TD	Time Delay
TL	Transmitter Laser
VCSELs	Vertical Cavity Surface Emitting Lasers
VSMR	Valley Signal to Mean Ratio
XP	X-Polarization
YP	Y-Polarization

Contents

Chapter 1

Introduction

1.1 Introduction

Information exchange is a major activity of our world and optical communication plays a vital role in the execution of the information exchange. Optical communication has revolutionized telecommunications industry. In optical communications systems an optical signal is used to carry information from one place to another. In this information age, one of the major issues is the secure transmission of information. Improvement of message security can potentially be achieved by using chaos.

Chaos is irregular and unpredictable, and two chaotic systems, starting from almost identical initial states, end in completely uncorrelated trajectories [1]. Hence it came as a surprise when Pecora and Carroll showed that two chaotic systems which are coupled by some of their internal variables can synchronize to a common identical chaotic motion [2]. The dynamics are still irregular and unpredictable, but both chaotic system have identical trajectories.

The combination of synchronization and unpredictability leads to an interesting application for secure communication. In 1992 Cuomo and Oppenheim [3] and Parlitz et al.[4] have demonstrated communication by synchronized chaotic electronic circuits. The research on the chaotic carrier generation in electrical circuits and optical devices has been started widely in the mid-1990s [5,6,7]. Most of these studies are based on the mixing of the message with a chaotic carrier and decoding them by subtracting the synchronization chaotic noise. In such schemes the message (M) is typically added to the chaotic carrier (C) so that the output is M+C. Through the achievement of chaos synchronization a replica of chaos C is generated by another chaotic system. By subtracting the synchronized chaos from the message added chaotic carrier the message is recovered: symbolically we have (M+C) – C = M.

Communication with the synchronized chaotic lasers has been demonstrated and widely studied. A suitable candidate for chaotic carrier generation using an optical device is a semiconductor laser [8, 9, 10]. Such a chaotic laser system and the synchronization of two lasers are discussed in section 1.3 and section 1.4 respectively.

The developments of the optical chaos communication using chaotic laser systems are as follows. In 1994 Colet and Roy proposed a scheme of digital communication using synchronized chaotic lasers. They used a single-mode Nd:YAG solid-state laser [5]. Information was encoded in the pulsed output of a chaotic Nd:YAG solid-state laser. A sinusoidal modulation of the cavity loss produces a pulsed output in which the occurrence time and the height of individual pulses is chaotic

Mirasso and Colet showed numerically that the synchronization of two semiconductor lasers is possible by injecting a part of output light from one laser to the other [11]. They showed that a message can be encoded in the chaotic carrier, transmitted by an optical fiber and decoded by a receiver.

VanWiggeren and Roy first demonstrated experimentally chaotic optical communications using erbium-doped fibre ring laser of wavelength 1.53 µm [6]. A 10 MHz message was encoded in the chaotic carrier and transmitted to the receiver system where message was decoded from the chaos carrier.

Sivaprakasam and Shore were the first to show experimentally synchronization and message encoding and decoding using chaotic external cavity semiconductor lasers [8, 9]. A 9.5 KHz square wave message was encoded and decoded successfully using the chaotic external cavity semiconductor lasers [9]. Subsequent work on optical communication with chaotic external cavity semiconductor lasers has been directed towards improving the message bandwidth and quality of recovered message [12-18].

A landmark result of communications using chaotic semiconductor lasers was reported in [16]. Argyris et al. set up a field experiment of optical chaos communication using a commercial optical network. The encoded message was transmitted over 120 km using chaotic transmitter laser. The message recovered using the synchronized receiver laser. The message transmitter rate was in the range of Giga bit per second with bit error rate (BER) below 10^{-7} was achieved.

The key idea that has been the focus of most research efforts is to generate a good replica signal at the receiver by exploiting the synchronization properties of the chaotic lasers. The quality of the decoded message from the chaotic carrier depends on the synchronization condition between the transmitter laser and the receiver laser. Laser operating conditions for high-quality synchronization and high-quality recovered message (signal-to-noise ratio) have been shown experimentally to be different [19]. In this thesis simulations are performed with the aim of identifying a regime of operation where the highest quality synchronization and the best message extraction are achieved simultaneously. Use of such an operating regime will facilitate practical deployment of optical chaos communications systems without the need for re-adjustment of laser operating conditions in the field.

1.2 Semiconductor Lasers

In 1960 a breakthrough came in the research area of the light sources. The laser was demonstrated as a bright, highly directed and coherent source of light. A laser is ideal of a single frequency and narrow linewidth. Two years later a semiconductor laser demonstrated. By now the semiconductor laser power conversion efficiencies of ~50% are common, whereas efficiencies of gas and solid-state laser are the order of 10%.

Semiconductor lasers have high efficiency, compact size, low cost and lifetime of several years. By now a large variety of semiconductor lasers are commercially available. Semiconductor lasers are used in such everyday items such as CD players, barcode readers, laser printers and laser scanners.

Semiconductor lasers are normally pumped by an injection current. The electrical pumping of the semiconductor lasers offers the versatility of direct current modulation. Due to fact that the semiconductor lasers can be directly modulated they are especially desirable optical sources for optical communication systems. Information can be impressed on the light output of semiconductor lasers via direct modulation of the bias current. External or indirect modulation may also be used for the same purpose.

Semiconductor lasers can easily be driven unstable by the use of optical feedback and in some cases the resulting output can be shown to follow a route to deterministic chaos [8, 9]. The impacts of optical feedback and optical injection on the laser dynamics are diverse. In such configurations the laser relaxation oscillation (RO) can become undamped and the laser starts behaving like an autonomous nonlinear oscillator. Additional bifurcations- that is, qualitative changes in the dynamics- may occur and destabilize the time-periodic dynamics into either quasiperiodiodicity or even chaos. When the laser exhibits such a rich and complex set of dynamical behaviours, the multimode emission can lead either to an apparently more regular total laser output or by contrast, can lead to a more complex laser chaotic dynamics of a higher dimension [20].

1.3 Semiconductor Lasers with Optical Feedback

A schematic diagram of a semiconductor laser subject to optical feedback is shown in fig.1.1. A plane mirror is used to reflect back a part of the light output of the laser into the laser cavity. The reflected light beam is called the optical feedback. The distance between the laser facet and the external mirror is defined as the external cavity length (*l*). R2 and R3 are the reflectivity of the mirrors. Fig.1.1 represents an external cavity laser system.

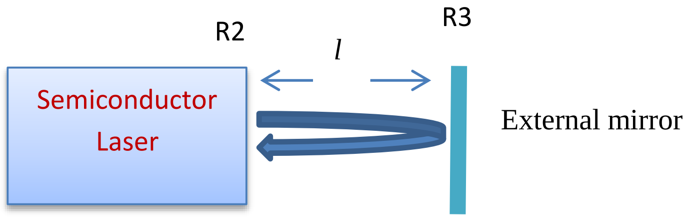

Fig.1.1. External cavity semiconductor laser system.

The external cavity length is an important parameter [21]. A semiconductor laser dynamical response may depend on the external cavity length and optical feedback strength. Tkach et al. [22] experimentally studied so-called ‘regimes of feedback’. Five operating regimes are now conventionally labelled ‘Regimes I to V’. Regime I with weak optical feedback strength, the laser line width can be either narrowed or broadened depending upon the phase of the optical feedback [23]. In Regime II longitudinal mode hopping can appear [24]. In Regime III the laser mode becomes stable and locked to minimum single-mode linewidth. Regime IV is termed the ‘coherence collapse’ regime. In this regime the laser linewidth broadens and the coherence length of the laser reduces dramatically [25]. The noise level is enhanced greatly under this condition. The effects in this regime are independent of the feedback phase. A further increase in the optical feedback strength leads the laser to Regime V. In this regime the laser achieves stable external cavity mode of operation. To reach the Regime V strong optical feedback is needed. So antireflection coating of the front facet of the laser is necessary. Fig.1.2 shows the regimes of feedback, which is a function of the feedback strength and distance of reflection. Fig.1.2 is taken from the reference [22]. Considerable effort has given to study the nature of the laser dynamics in the coherence collapse regime [25]. Cho and Umeda have studied the relation between coherence collapse and chaotic dynamics of an external cavity semiconductor laser [26]. In Regime IV, the presence of chaotic dynamics in an external cavity laser system has an important potential application in secure optical communications.

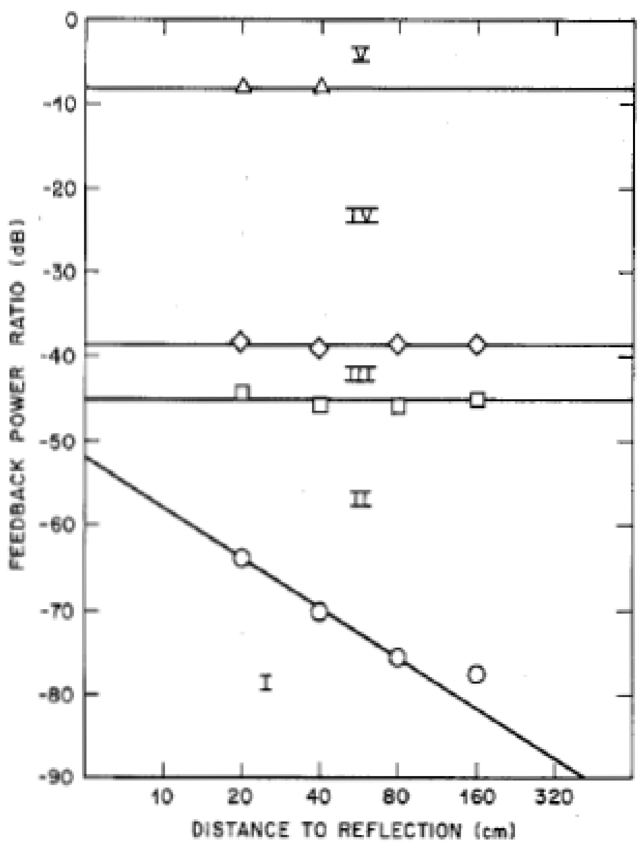

Fig.1.2. Plot showing the power levels at which the transitions between regimes occur, as a function of distance to the reflection. From [22].

1.4 Optical Chaos Communications

An optical chaos communications system consists of a transmitter, a transmission line, and a receiver, these three elements can be common to all communication systems. A schematic diagram of an optical chaos communications system is shown in fig.1.3 [10]. The transmission of encrypted messages can be achieved using a semiconductor laser. The chaos generator in fig.1.3 is an external cavity semiconductor laser. The external cavity semiconductor laser is defined as the transmitter laser (TL). A message can be embedded in a chaotic carrier optical signal generated by direct bias current modulation of a chaotic semiconductor laser. A schematic diagram of message embedding is shown in fig.1.4.

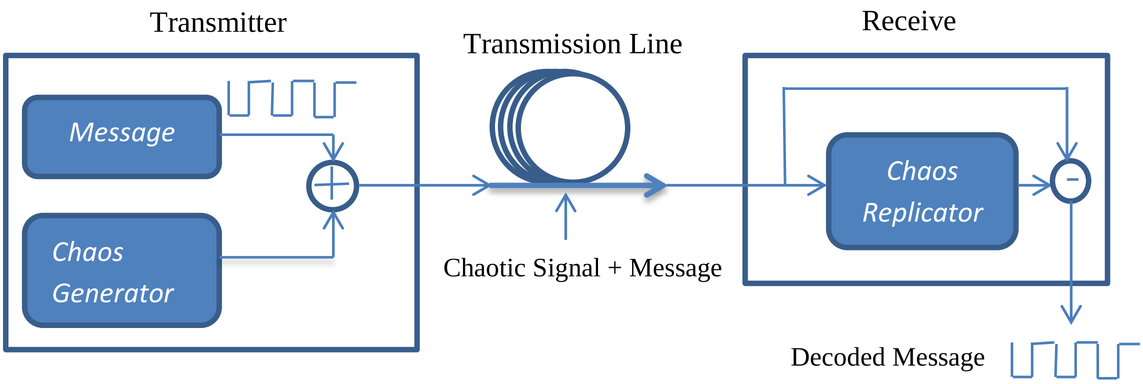

Fig.1.3. A Schematic diagram of optical chaos communication system. From reference [10].

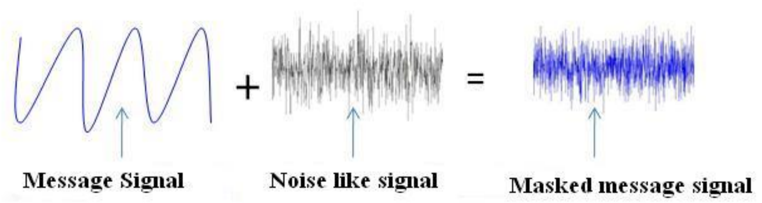

Fig.1.4. A Schematic diagram of message embedding.

At the receiver the message is recovered with the help of a chaos replicator. A chaos replicator is a semiconductor laser subject to the optical injection from the transmitter laser. The chaotic replicator in fig. 1.3 is defined as receiver laser (RL). The receiver laser is chosen to be as identical as possible to the transmitter laser in order to achieve the chaotic synchronization. Chaotic synchronization of the transmitter and receiver laser is key to the use of optical chaos in communications [5, 6, 8, 9]. The term 'chaotic synchronization' refers to a variety of phenomena in which coupled chaotic systems adjust their dynamics to achieve common behaviour [27].

The TL and the RL are unidirectionally coupled. Two lasers are coupled unidirectionally if the dynamics of one laser (TL) influences the dynamics of other (RL), and TL is isolated from the RL, so that the dynamics of the RL does not affect the dynamics of the TL. A schematic diagram of the unidirectional coupled system is shown if fig. 1. 5.

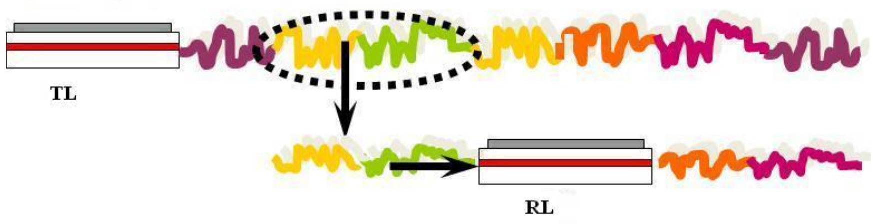

Fig. 1.5. A schematic diagram of unidirectionally coupled TL and RL

The message is recovered by subtracting the synchronized chaotic signal output of the receiver laser from the masked message chaotic signal of the transmitter laser. A schematic diagram of a message recovery is shown in fig. 1.6. The message can be successfully recovered if the RL output is well synchronized to the TL.

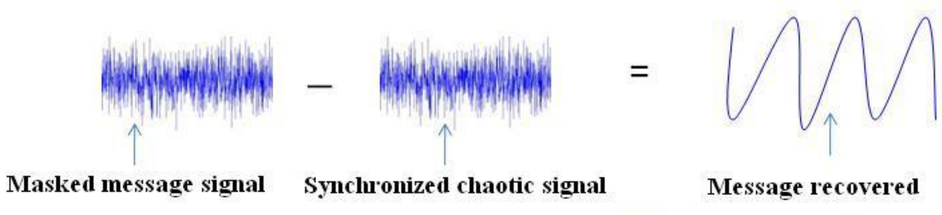

Fig.6. A Schematic diagram of message recovery.

1.5 Time Delay in a Chaotic Semiconductor Laser

The external cavity round trip time of the external cavity semiconductor laser system is called the time delay (TD) in the laser dynamics. Time delay concealment may be regarded as an additional key to encode messages in optical chaos communication [28]. Rontani et al. have theoretically investigated TD identification using auto-correlation function and mutual information methods [28]. Time delay concealment has been studied numerically and experimentally [29-31]. In chapter 5 time delay concealment is explored experimentally in a scheme of optical feedback incorporating variation of the polarization-angle of optical feedback into the Vertical-Cavity Surface-Emitting Laser.

1.6 Thesis Outline

Chapter 2 describes the Lang-Kobayashi model which is used to describe the dynamical behaviour of external cavity semiconductor lasers. This model includes the open loop and the close loop configuration. Langevin noise is also discussed. Cross correlation function is also discussed in this chapter. The cross correlation function is used to calculate the synchronization quality between the transmitter laser and the receiver laser. The Fourier transform is discussed as a means to calculate the signal to noise ratio of the recovered message.

Chapter 3 discusses optical chaos communications using analogue message modulation. The chapter explores the effects of bias current, modulation frequency and coupling strength on the synchronization between the transmitter laser and the receiver laser. The effects of bias current, modulation frequency and coupling strength on the quality of encoded message. Variations of the synchronization with respect to bias current and modulation frequency are shown using contour plots. Optimum conditions for synchronization and quality of recovered message are identified.

Chapter 4 discusses digital optical chaos communications. The effect of bias current, digital message modulation rate and coupling strength on the synchronization between the transmitter and receiver laser is studied in this chapter. The quality of the decoded message is defined via calculations of the Bit Error Rate (BER). The effect of bias current, digital message modulation rate and coupling strength on the BER of subtracted message are discussed. The operating conditions for the best synchronization and the best BER are studied.

Chapter 5 describes auto-correlation and the permutation entropy methods to analyze the time delay signature in the output intensity of the external cavity VCSELs. A time delay signature appears due to the external cavity. Time delay identification is studied as a function of bias current of the VCSELs, optical feedback and the polarization angle of the feedback. This chapter describes time delay concealment which can be achieved at certain condition of the polarization angle of the optical feedback.

Chapter 6 summarises the research work

References

[1] H. G. Schuster and W. Just., Deterministic Chaos. Wiley-VCH, Weinheim, 2005.

[2] L. M. Pecora and T.L. Carroll, "Synchronization in chaotic systems", Phys. Rev. Lett., Vol. 64, pp. 821–824, 1990.

[3] K. M. Cuomo and A. V. Oppenheim, "Circuit implementation of synchronized chaos with applications to communications", Phys. Rev. Lett., vol. 71, pp. 65–68, 1993.

[4] L. Kocarev, K. S. Halle, K. Eckert, L. O. Chua and U. Parlitz, "Experimental demonstration of secure communications via chaotic synchronization", Int. J. Bifurcation Chaos, Vol. 02, Issue 03, pp. 709-714, Sep. 1992.

[5] P. Colet and R. Roy, "Digital communication with synchronized chaotic lasers", Opt. Lett., vol.19, pp. 2056, 1994.

[6] G. D. VanWiggeren and R. Roy, "Communication with Chaotic Lasers", Science, vol. 279, pp. 1200, 1998.

[7] G. D. VanWiggeren and R. Roy, "Optical Communication with Chaotic Waveforms", Phys. Rev. Lett., vol. 81, pp. 3547, 1998.

[8] S. Sivaprakasam and K. A. Shore, "Demonstration of optical synchronization of Chaotic external laser diode", Opt. Lett.vol. 24, pp.466-468, 1999.

[9] S. Sivaprakasam and K. A. Shore, "Message encoding and decoding using chaotic external-cavity diode lasers", IEEE J. Quantum Electron., vol. 36, pp. 35–39, 2000.

[10] D. M. Kane and K. A. Shore (Editors), Unlocking Dynamical Diversity: Optical Feedback Effects on Semiconductor Lasers, John Willey & Sons, Ltd, 2005.

[11] C. R. Mirasso, P. Colet, and P. Garc´ıa-Fern´andez, “Synchronization of chaotic semiconductor lasers: Application to encoded communications”, IEEE Photon. Technol. Lett., vol. 8, pp. 299–301, 1996.

[12] J. Paul, P. S. Spencer, S. Sivaprakasam and K. Alan Shore, “GHz Bandwidth Message Transmission Using Chaotic diode Lasers”, Elec. Lett., vol. 38, pp. 28-29, 2001.

[13] I. Fischer, Y. Liu, and P. Davis, “Synchronization of chaotic semiconductor laser dynamics on subnanosecond time scales and its potential for chaos communication”, Phys. Rev. A, vol. 62, pp. 011801, 2000.

[14] M. W. Lee, J. Paul, S. Sivaprakasam and K. A. Shore , “Comparison of closed-loop and open-loop feedback schemes of message decoding using chaotic laser diodes”, Opt. Lett., vol. 28, pp. 2168-2170, 2003.

[15] J. Paul, M. W. Lee, and K. A. Shore, “3.5-GHz signal transmission in an all-optical chaotic communication scheme using 1550-nm diode lasers”, IEEE Photon. Technol. Lett., vol. 17, pp. 920–922, 2005.

[16] A. Argyris, D. Syvridis, L. Larger, V. Annovazzi-Lodi, P. Colet, I. Fischer, J. García-Ojalvo, C. R. Mirasso, L. Pesquera, and K. A. Shore, “Chaos-based communications at high bit rates using commercial fiberoptic links”, Nature, vol. 437, pp. 343–346, 2005.

[17] V. Annovazzi-Lodi, M. Benedetti, S. Merlo, M. Norgia, and B. Provinzano, “Optical chaos masking of video signals”, IEEE Photon. Technol. Lett., vol. 17, pp. 1995–1997, 2005.

[18] D. Kanakidis, A. Argyris, A. Bogris, and D. Syvridis, “Influence of the decoding process on the performance of chaos encrypted optical communication systems”, J. Lightw. Technol., vol. 24, pp. 335–341, 2006.

[19] Y. Hong, M. W. Lee, and K. A. Shore, “Optimised Message Extraction in Laser Diode Based Optical Chaos Communications”, IEEE J.Quant. Electron., vol. 46, 2010.

[20] K. Ludge (editor), Nonlinear laser dynamics from quantum dots to cryptography by Kathly Ludge, Wiley- VCH Verlag GmbH & Co. KGaA, Germany 2012.

[21] O. Hirota and Y. Suematsu, “Noise properties of injection lasers due to reflected waves”, IEEE J. Quant. Electron., vol. 15, pp. 142-149, 1979.

[22] R. W. Tkach and A.R. Chraplyvy, “Regimes of feedback effects in 1.5-µm distributed feedback lasers”, IEEE J. Lightwave Technology, vol. 4, pp. 1655-1661, 1986.

[23] K. Kikuchi and T. Okoshi: “Simple formula giving spectrum-narrowing ratio of semiconductor-laser output obtained by optical feedback”, Electron. Lett., vol. 18, pp. 10-12, 1982.

[24] R. W. Tkach and A. R. Chraplyvy, “Line broadening and mode splitting due to weak feedback in single frequency 1.5-pm lasers”, Electron. Lett., vol. 21, pp. 1081-1083, 1985.

[25] D. Lenstra, B. H. Verbeek, and A. J. Den Boef, “Coherence collapse in single mode semiconductor lasers due to optical feedback”, IEEE J. Quantum Electron., vol. QE-21, pp. 674-679, 1985.

[26] Y. Cho and T. Umeda, “Observation of chaos in a semiconductor laser with delayed feedback”, Opt. Commun., vol. 59, pp.131-136, 1986.

[27] S. Boccaletti, J. Kurths, G. Osipov, D.L. Valladares and C.S. Zhou, “The synchronization of chaotic systems”, Phys. Reports, vol 366, pp 1-101, Aug. 2002.

[28] D. Rontani, A. Locquet, M. Sciamanna, D. S. Citrin, and S. Ortin, “Time-delay identification in a chaotic semiconductor laser with optical feedback: a dynamical point of view”, IEEE J. Quantum Electron., vol. 45, pp. 879–891, 2009.

[29] N. Li, W. Pan, S. Xiang, L. Yan, B. Luo, X. Zou, L. Zhang and P. Mu, “Photonic Generation of Wideband Time-Delay-Signature-Eliminated Chaotic Signals Utilizing an Optically Injected Semiconductor Laser”, IEEE J. Quantum Electron., vol. 48, pp. 1339–1345, 2012.

[30] J. Wu, Z. Wu, X. Tang, X. Lin, T. Deng, G. Xia and G. Feng, “Simultaneous Generation of Two Sets of Time Delay Signature Eliminated Chaotic Signals by Using Mutually Coupled Semiconductor Lasers”, IEEE Phot. Technol. Lett., vol. 23, pp. 759-761, 2011.

[31] S. Xiang, W. Pan, B. Luo, L. Yan, X. Zou, N. Jiang, L. Yang, H. Zhu, “Conceal time-delay signature of chaotic vertical-cavity surface-emitting lasers by variable-polarization optical feedback”, Optics Communications, vol. 284, pp. 5758-5765, 2011.

Chapter 2

Numerical Modelling of Semiconductor Laser Optical Chaos Communications Systems

2.1 Introduction

The application of the semiconductor laser in optical chaos communications is the focus of this thesis. Numerical modelling of a semiconductor laser-based optical chaos communication system; synchronization of a transmitter-receiver laser system and signal to noise ratio of transmitted signal are discussed in this chapter.

Unintentional external feedback from the fibre facet in a semiconductor laser-to-fibre coupling system is a serious problem. External feedback degrades the modulation characteristics and increases the intensity noise in transmitted signals [1-4].

But there may be also beneficial effects of external optical feedback on the laser performance. For example optical feedback enhanced spontaneous emission and spectral line narrowing of the laser [5]. The dynamical response of semiconductor lasers is highly nonlinear, and semiconductor lasers can easily be driven into chaotic dynamics [6]. Lang and Kobayashi published a paper [7] on the dynamics of semiconductor lasers subject to external optical feedback. The analysis of many semiconductor laser-based optical chaos communication systems can be accomplished using the Lang-Kobayashi model.

2.2 Lang Kobayashi Model of External Cavity Semiconductor Laser

The Lang-Kobayashi model describes the effect of an optical feedback on a single mode semiconductor laser [7]. A schematic diagram of an external cavity semiconductor laser is shown in fig.2.1. An external mirror is used to provide external optical feedback to a semiconductor laser. R2 and R3 are the mirror reflectivity. τ_{ex} is the external cavity round trip time. In this model a single reflection from the external mirror is taken into account.

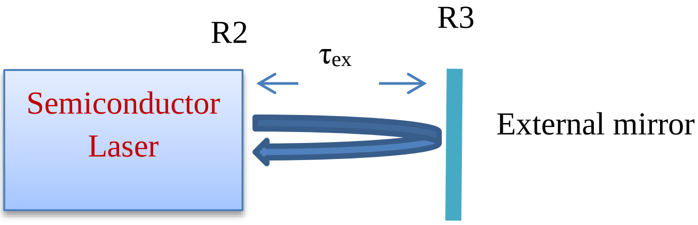

Fig.2.1. Schematic diagram of an external cavity semiconductor laser system.

The Lang-Kobayashi rate equations for the complex electric field and carrier numbers in the laser are given by [6, 7]:

$$\frac{dE(t)}{dt} = \frac{1}{2}(1+i\alpha)\left[G(t) - \frac{1}{\tau_p}\right]E(t) + \kappa E(t-\tau_{ex})e^{-i\omega\tau_{ex}} \quad (2.1)$$

$$\frac{dN(t)}{dt} = \frac{I}{e} - \frac{N(t)}{\tau_N} - G(t)|E(t)|^2 \quad (2.2)$$

$$G(t) = \frac{g_o(N(t) - N_o)}{1 + \varepsilon|E(t)|^2} \quad (2.3)$$

Here E(t) is the electrical field inside the laser cavity; τ_{ex} is the external cavity round trip time; τ_N is the carrier life time; τ_P is the photon life time ; e is the electronic charge; α is the linewidth enhancement factor; N(t) is the carrier number; N_0 is the carrier number at transparency; G(t) is the gain in cavity; g_0 is the linear gain coefficient; ε is the gain saturation coefficient; κ is the external mirror feedback rate. The last term in eq. (2.1) represents the external feedback. The feedback rate, κ is related to cavity parameters as [6]

$$k = f(1-R_2)\left(\frac{R_3}{R_2}\right)^{\frac{1}{2}}\frac{c}{2l} \quad (2.4)$$

Where c is the speed of light; *l* is the optical length of the laser cavity; R_2 is the power reflectivity of the laser facet facing the external mirror, R_3 is the power reflectivity of the external mirror and *f* is the fraction of the reflected field which couples back into the lasing mode [6].

2.3 Transmitter-Receiver Laser Optical Chaos Communication Configuration

In a typical optical chaos communication system a transmitter laser (TL)-receiver laser (RL) configuration is used. There are two types of configurations namely 'closed loop' and 'open loop' which are discussed in the following sub-sections. In these configurations the transmitter laser is subject to external feedback. A message for transmission may be added by modulating the bias current of the transmitter laser. Synchronization between the TL and the RL can be achieved when a small fraction of the light output from transmitter laser is injected into the receiver laser. The message decoding is achieved by subtracting the synchronized output of the RL from the TL output signal.

2.3.1 Closed Loop Transmitter-Receiver Laser Configuration

A schematic diagram of the configuration is shown in fig. 2.2 where it is seen that both the transmitter and the receiver laser are subject to optical feedback from an external mirror. Unidirectional coupling is enabled between the lasers so that the transmitter laser affects the receiver laser but not vice versa. An optical isolator is used to achieve the unidirectional coupling from the TL to the RL. The receiver laser is subject to its own external feedback and also to optical injection from the transmitter laser.

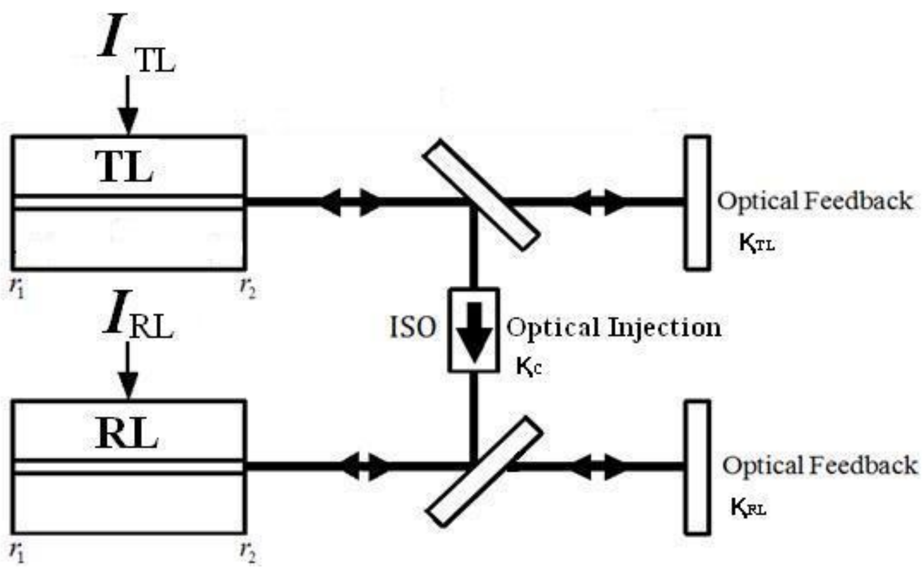

Fig. 2.2. Schematic diagram of optical chaos communication closed loop transmitter-receiver configuration.

2.3.2 Open Loop Transmitter-Receiver Laser Configuration

In an open loop transmitter-receiver laser configuration the receiver laser is not subject to external feedback. A schematic diagram of the open loop transmitter-receiver laser configuration is shown in fig. 2.3.

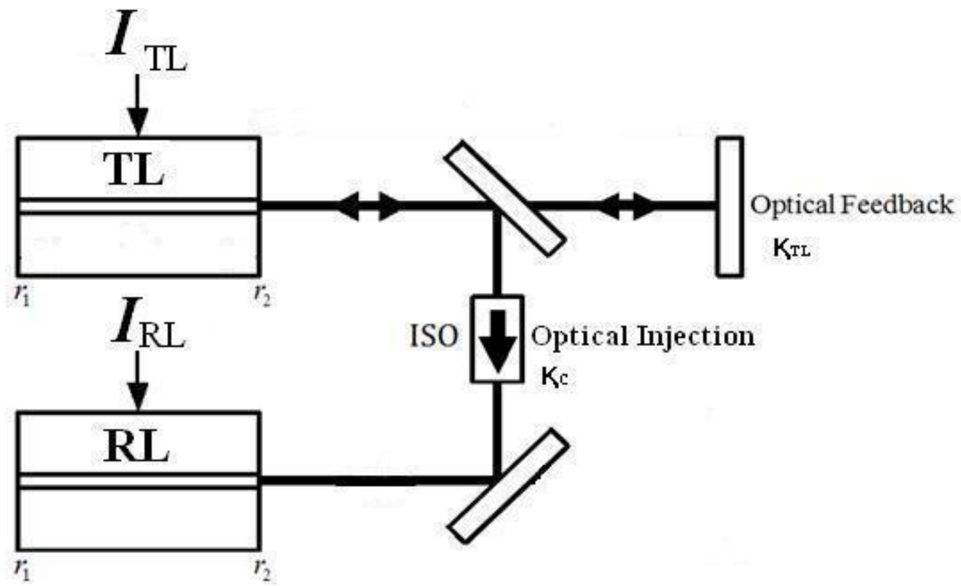

Fig. 2.3. Schematic diagram of open loop transmitter-receiver optical chaos communication configuration.

The advantage of the closed loop configuration in comparison to the open loop configuration is that, the closed loop configuration leads to better synchronization than the open loop configuration [8]. The disadvantage of the closed loop configuration is the need to maintain careful alignment of the several optical components.

2.4 Optical Chaos Communication using Analogue Modulation

The open loop transmitter-receiver laser configuration (fig. 2.3) is studied in this scheme. An optical chaotic carrier is generated using optical feedback in semiconductor lasers.

An analogue message is generated using direct current modulation of the TL. The analogue sinusoidal message is modulated as:

$$I_{TL} = I_{dc}(1 + h\sin(\omega t)) \tag{2.5}$$

Here I_{dc} is the bias current of the transmitter laser, h is the modulation depth and ω is the modulation frequency. The receiver laser is driven at a constant current, with no modulation.

The Lang-Kobayashi external cavity semiconductor laser model is used in the simulation of this configuration from equations 2.1 - 2.3.

$$\frac{dE_{TL}(t)}{dt} = \frac{1}{2}(1+i\alpha)\left[G_{TL}(t) - \frac{1}{\tau_p}\right]E_{TL}(t) + \kappa_{TL}E_{TL}(t-\tau_{ex,TL})e^{-i\omega_{TL}\tau_{ex,TL}} \quad (2.6)$$

$$\frac{dE_{RL}(t)}{dt} = \frac{1}{2}(1+i\alpha)\left[G_{RL}(t) - \frac{1}{\tau_p}\right]E_{RL}(t) + \kappa_c E_{TL}(t-\tau_c)e^{i\Delta\omega t} \quad (2.7)$$

$$\frac{dN_{TL,RL}(t)}{dt} = \frac{I_{TL,RL}}{\mathrm{e}} - \frac{N_{TL,RL}(t)}{\tau_N} - G_{TL,RL}(t)\left|E_{TL,RL}(t)\right|^2 \quad (2.8)$$

$$G_{TL,Rl}(t) = \frac{g_o(N_{TL,RL}(t) - N_o)}{1 + \varepsilon\left|E_{TL,RL}(t)\right|^2} \quad (2.9)$$

Here the indices TL and RL refer to the transmitter laser and the receiver laser respectively E_{TL} (E_{RL}) is the electric field and N_{TL} (N_{RL}) is the carrier number; κ_{TL} is the transmitter laser feedback rate κ_c is the coupling strength from the TL to the RL. The time taken by the light to travel from the TL to the RL is called the time of flight τ_C. $\Delta\omega = \omega_{TL} - \omega_{RL}$ is the frequency detuning between the TL and the RL.

2.5 Optical Chaos Communication using Digital Modulation

Direct current modulation of the TL is again used in this case. A binary random bit sequence (BRBS) message is impressed via the transmitter laser drive current. The BRBS is a uniformly distributed random bit sequence of zeros and ones. The TL drive current is modulated as:

$$I_{TL} = I_{dc}(1 + h(\mathrm{BRBS})) \quad (2.10)$$

Here I_{dc} is the bias current of the transmitter laser and h is the modulation depth.

The Lang-Kobayashi model [7] is used to simulate the open loop transmitter -receiver laser configuration including Langevin noise. The last terms of eq.(2.11) and eq.(2.12) are the Langevin noise terms for the laser system. Where β is spontaneous emission factor. Langevin noise is discussed in the next section.

$$\frac{dE_{TL}(t)}{dt} = \frac{1}{2}(1+i\alpha)\left[G_{TL}(t) - \frac{1}{\tau_p}\right]E_{TL}(t) + \kappa_{TL}E_{TL}\left(t-\tau_{ex,TL}\right)e^{-i\omega_{TL}\tau_{ex,TL}} + \sqrt{\frac{2\beta N(t)}{\tau_N \Delta t}}\gamma_{TL}(t) \quad (2.11)$$

$$\frac{dE_{RL}(t)}{dt} = \frac{1}{2}(1+i\alpha)\left[G_{RL}(t) - \frac{1}{\tau_p}\right]E_{RL}(t) + \kappa_c E_{TL}(t-\tau_c)e^{i\Delta\omega t} + \sqrt{\frac{2\beta N(t)}{\tau_N \Delta t}}\gamma_{RL}(t) \quad (2.12)$$

$$\frac{dN_{TL,RL}(t)}{dt} = \frac{I_{TL,RL}}{\mathrm{e}} - \frac{N_{TL,RL}(t)}{\tau_N} - G_{TL,RL}(t)\left|E_{TL,RL}(t)\right|^2 \quad (2.13)$$

$$G_{TL,RL}(t) = \frac{g_o(N_{TL,RL}(t) - N_o)}{1 + \varepsilon\left|E_{TL,RL}(t)\right|^2} \quad (2.14)$$

2.6 Langevin Noise and Digital Message Transmission

The original Langevin equation [9] was used to describe Brownian motion, the apparently random movement of a particle in a fluid due to collisions with the molecules of the fluid. Such collisions provide a force which drives the particle in random directions. From a mathematical viewpoint the key feature of the Langevin equation is that the random force is directly added to the equation of motion.

In semiconductor lasers the analogue of the random Langevin force is spontaneous emission which adds photons with random phases to the laser emission. The spontaneous emission thus appears as random noises which add directly to the light emission [10] and is thus termed Langevin noise. Langevin noise is prescribed using means and correlations which encapsulate the underlying randomness of the spontaneous emission process. Thus a Langevin noise source having a time dependence f(t) possesses the following generic properties:

The average value over time is zero: $\langle f(t) \rangle = 0$.

Considering the noise source at different times ,say f(t) and f(t-τ) the correlation function $\langle f(t)f(t-\tau)\rangle$ exhibits a delta function behaviour: $\langle f(t)f(t-\tau)\rangle = \delta(\tau)$.

The delta function is a real valued function, which value is infinity at origin and zero everywhere.

$$\delta(x) = \begin{cases} +\infty, & x = 0 \\ 0, & x \neq 0 \end{cases} \tag{2.15}$$

The emission of the photon is associated with the recombination of an electron and hole pair in the semiconductor and hence a Langevin noise term will also appear in the rate equation describing the dynamics of the carrier density or number [10]. In this way using the Langevin approach the carrier density rate equation takes the form:

$$\frac{dn}{dt} = \frac{I}{e} - \frac{n}{\tau_s} - g(n)S + f(t) \tag{2.16}$$

The Langevin noise term [11] $f(t) = \frac{v_e}{\sqrt{\Delta t}}\chi_e$ (2.17)

Where χ_e is a Gaussian random variable, which is uniformly distributed over the interval [0, 1]. A random variable is a variable whose value is subject to variations due to chance. It can take on a set of possible different values, each with an associated probability. Noise is generated in a system by the photon emission perturbation. Δt is the step size of the computer simulation.

$$v_e = \sqrt{\frac{2\beta n(t)}{\tau_N}} \tag{2.18}$$

Where β is the spontaneous emission factor, $n(t)$ is the carrier number and , τ_N is the carrier lifetime.

It appears that the Langevin noise term in [12] is dimensionally incorrect due to the omission of the time step. The correct form of Langevin noise is derived in [10].

2.7 Synchronization

Synchronization is a process where two or more systems interact with each other and show identical dynamical behaviour. For example, cells in the heart beat together.

Cuomo and Oppenheim [13] first reported pioneering work on the synchronization of two chaotic systems. The synchronization of chaotic systems and their practical approach in secure communication has been studied extensively in [14].

Several approaches have been proposed to determine the quality of synchronization such as (i) synchronization diagram, (ii) mutual information (discussed in chapter 5) and (iii) cross correlation function (discussed in the next section).

A synchronization diagram can show the quality of synchronization of the system. The TL and the RL are coupled back to back, so the time of flight is zero. The synchronization diagram of a back to back coupled TL and RL is illustrated in fig.2.4. The intensities of the TL I_{TL}(t) and the RL I_{RL}(t) at the same time are plotted on x-axis and y-axis respectively in fig.2.4.

When the RL output intensities are varying same as the variation of the TL output intensities, the plot of the RL output intensity vs. TL output intensities will be straight line with 45^0 slope. In fig.2.4 the synchronization diagram appears (approximately) straight line with 45^0slope.

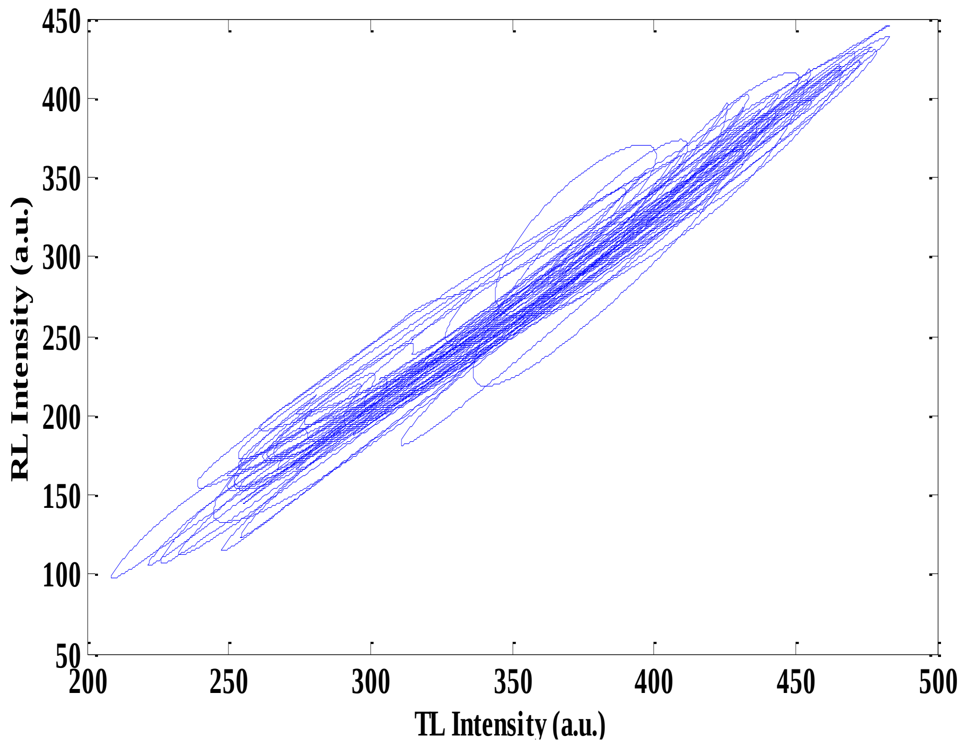

Fig.2.4. RL intensity vs. TL intensity.

2.7.1 Cross Correlation between the Transmitter Laser and the Receiver Laser

The cross correlation method estimate the quality to which two systems are synchronized. Suppose X(i) and Y(i) (where i may be used to 1, 2,…….., N.) are the sampled output intensities of the TL and the RL respectively. To calculate the cross correlation between the TL and the RL, the RL intensities Y(i) shifted by d data points. The shift d is defined as the delay between the TL and the RL. The cross correlation, C, is defined as:

$$C = \frac{\sum_{i=0}^{N-1}[(X(i) - \langle X \rangle) \times (Y(i-d) - \langle Y \rangle)]}{\sqrt{\sum_{i=0}^{N-1}(X(i) - \langle X \rangle)^2}\sqrt{\sum_{i=0}^{N-1}(Y(i-d) - \langle Y \rangle)^2}} \qquad (2.19)$$

Where <X> and <Y> are the average of the X(i) and the Y(i) respectively.

An example of cross correlation is shown in the fig. 2.5. Cross correlation is calculated using eq. (2.19) and is plotted as function of d. The output intensities of the TL and the RL are sampled at 0.125×10^{-12} s. The cross correlation are calculated for d from -1ns to +1ns at the increments of 0.01ns. In fig.5 cross correlation vs. delay d is plotted.

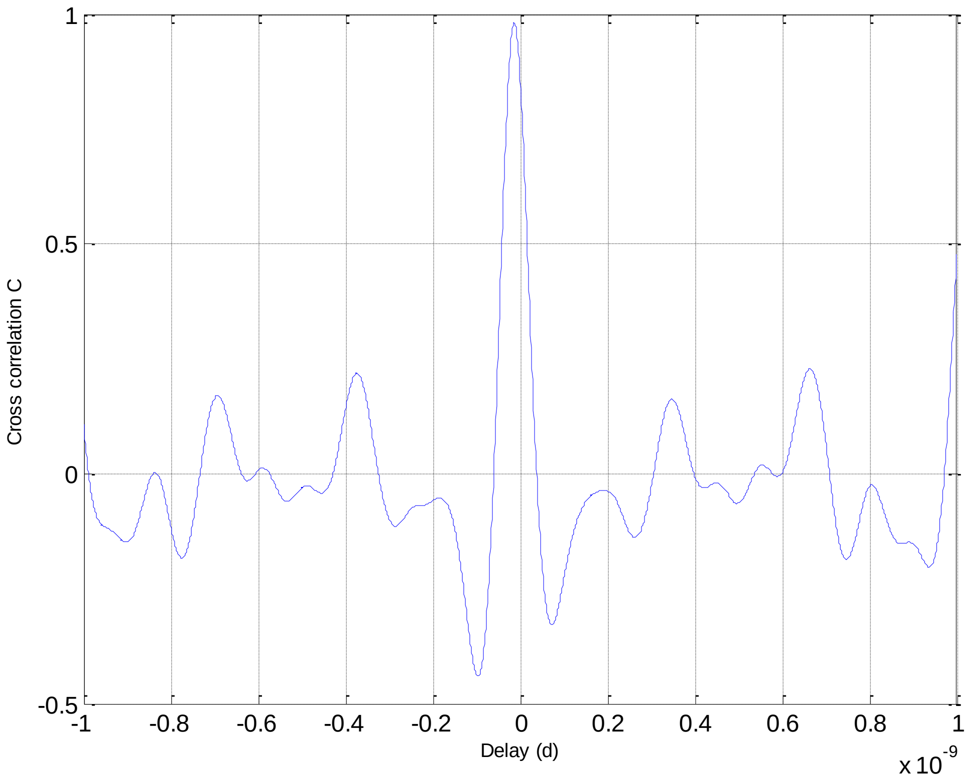

Fig. 2.5. Cross correlation between TL and RL vs. delay.

For the TL-RL coupled system two types of synchronization can be identified. One is called perfect or complete synchronization which occurs when two lasers are coupled in such a way that the TL optical feedback rate is equal to the sum of the RL optical feedback rate and the optical coupling rate from the TL. In addition the TL and the RL external cavity round trip time should be the same. Under these conditions the RL output $I_{RL}(t)$, synchronizes with TL output $I_{TL}(t-\tau_c+\tau_{ext})$, where τ_C is the time of flight from the TL to the RL and τ_{ext} is external cavity round trip time [15, 16].

The second type of synchronization which is commonly observed is so-called injection-locking or general synchronization [8, 17]. In this case the RL output $I_{RL}(t)$ synchronizes with the TL output $I_{TL}(t-\tau_c)$, where τ_c is the time of flight from the TL to the RL.

In 2006, S.Peters-Flynn et al. demonstrated that the maximum correlation does not necessarily occur at one of these two $d=\tau_c$ or $d=\tau_c-\tau_{ext}$ in certain special circumstances [18].They showed that the maximum correlation is also depend on the injection power between the TL and the RL [18]. Fig.2.6 shows the correlation as function of the injection rate between the TL and the RL. It is seen in fig. 2.6 the cross correlation is decreases for coupling rate 20ns^{-1} to 30ns^{-1} and then after coupling rate 30ns^{-1} cross correlation increases.

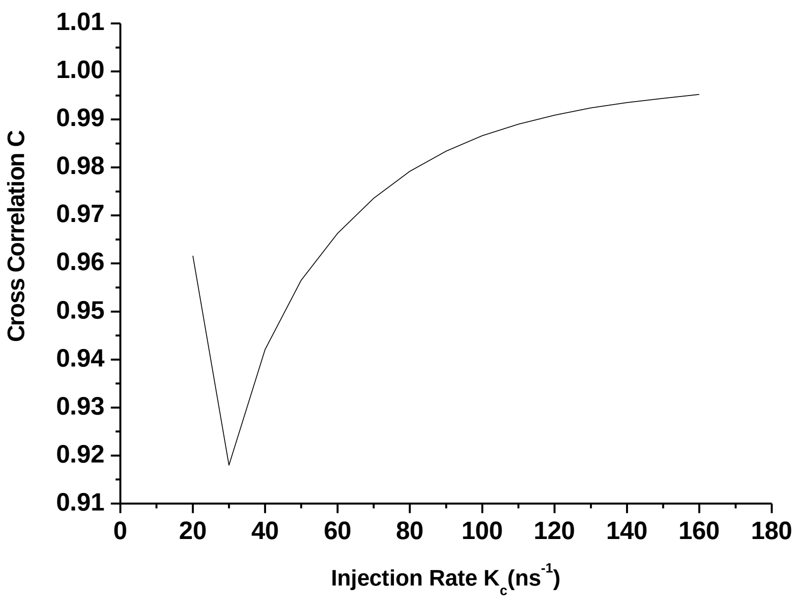

Fig.2.6. TL-RL cross correlation(C) vs. injection rate K_c.

2.8 Fourier Transform

In the 19th century Joseph Fourier gave a mathematical formula which transforms a time domain function into a frequency domain function.

Let *f(t)* is a continuous function of a real variable time t. The Fourier transform of the *f(t)* is defined as:

$$F(\omega) = \int_{-\infty}^{+\infty} f(t)e^{-i\omega t}\,dt \tag{2.20}$$

Where ω is the frequency variable. $f(t)e^{-i\omega t}$ is a complex valued function of t. The integral of this function gives a complex valued function. Which can be expressed as: *F*(ω) = R(ω)+ *i*I(ω). Where R(ω) is the real part and I(ω) is the imaginary part.

The magnitude $|F(\omega)| = \sqrt{R^2(\omega) + I^2(\omega)}$ is called the Fourier spectrum of *f(t)*. The square of the spectrum $|F(\omega)|^2 = R^2(\omega) + I^2(\omega)$ is called the power spectrum of *f(t).*

The Fourier transform is applicable to continuous time functions. A discrete-time version of the Fourier Transform is given to perform the spectral analysis on discrete time function. This is called Discrete-Time Fourier Transform (DTFT).

The transform can be written as:

$$X(e^{i\omega}) = \sum_{n=0}^{N-1} x[n]e^{-in\omega} \tag{2.21}$$

Where N is the length of the signal *x[n]*. Note that in this transform ω is a continuous variable.

If the frequency is sampled in the frequency domain to give discrete frequencies $\omega = \frac{2\pi k}{N}$. Where *k* = 0, 1, 2, …, N-1.

Then the transform is called the Discrete Fourier Transform (DFT) [19]:

$$X_D[k] = X\left(e^{\frac{i2\pi k}{N}}\right) = \sum_{n=0}^{N-1} x[n]e^{\frac{-i2\pi kn}{N}} = \sum_{n=0}^{N-1} x[n]W^{kn} \tag{2.22}$$

Where W= $e^{\frac{-i2\pi}{N}}$ and k is the discrete frequency variable. This transform is periodic in N.

Eq.(2.22) requires N complex multiplications for each of N frequencies. So the evaluations of the N^2 complex multiplication are performed. The computer will take a long time to evaluate N^2 multiplication and addition of the complex numbers. A number of algorithms have been designed to reduce this number and therefore increase the processing speed. Hence an efficient computer algorithm has been developed. This is known as Fast Fourier Transform (FFT). FFT makes the number of complex multiplication and addition proportional to $Nlog_2 N$. The FFT algorithm is not discussed here. Matlab software is used to perform the FFT of the signal in this study.

2.9 Signal to Noise Ratio

The FFT is used to calculate the signal to noise ratio (SNR). Signal to noise ratio is the message quality measure of the recovered message at the receiver end of analogue optical chaos communication systems.

FFT is performed on the samples *I[n]* of the output intensity of the receiver laser. P_S, the signal power, is defined as the absolute value of the spectral component at the message modulation frequency. $<P_N>$, the average noise power, is defined as the average value of all spectral components (except the message modulation frequency) of the FFT spectrum. The FFT components P[k] are given from eq.(2.22) as:

$$P[k] = \sum_{n=0}^{N-1} I[n]W^{kn}$$

It is noted that $P_S = |P[k]|_{k=S}$.

$$< P_N > = \frac{1}{N-1}\sum_{k} |P[k]| , k \in \{0,1,2, \dots \dots , N-1 \backslash S\}$$

The SNR is defined as:

$$SNR = \frac{P_S}{< P_N >} \qquad (2.23)$$

The Bit Error Rate (BER) is used to measure the message quality of the recovered message in digital optical chaos communication systems, which is studied in chapter 4.

References

[1] R. F. Broom, E. Mohn, C. Risch, and R. Salathe, “Microwave self-modulation of a diode laser coupled to an external cavity,” IEEE J. Quantum Electron., vol. 6, pp. 328-334, June 1970.

[2] T. Morikawa, Y. Mitsuhashi, and J. Shimada, “Return-beam induced oscillations in self-coupled semiconductor lasers,” IET J. Electron. Lett., vol. 12, pp. 435-436, Aug. 1976.

[3] I. Ikushima and M. Maeda, “Self-coupled phenomena of semiconductor lasers caused by an optical fiber,” IEEE J. Quantum Electron., vol. 14, pp. 331-332, May 1978.

[4] N. Chinone, K. Aiki, and R. Ito, “Stabilization of semiconductor laser outputs by a mirror close to a laser facet,” Appl. Phys. Lett., vol. 33, pp. 990-992, Dec. 1978.

[5] L. Goldberg, H. F. Taylor, A. Dandridge, J. F. Weller, and R. O. Miles, “Spectral characteristics of semiconductor lasers with optical feedback,” IEEE J. Quantum Electron., vol. 18, pp. 555-564, Apr. 1982.

[6] D. M. Kane and K. A. Shore (Editors), Unlocking Dynamical Diversity: Optical Feedback Effects on Semiconductor Lasers, John Willey & Sons, Ltd, 2005.

[7] R. Lang and K. Kobayashi, “External optical feedback effects on semiconductor injection laser properties,” IEEE J. Quantum Electron., vol. 16, pp. 347-355, 1980.

[8] A. Locquet, C. Masoller, and C. R. Mirasso, “Synchronization regimes of optical-feedback-induces chaos in unidirectionally coupled semiconductor lasers,” Phys. Rev. E, vol. 65, 056205, 2002.

[9] P. Langevin, “On the Theory of Brownian Motion,” C. R. Acad. Sci. (Paris) 146, pp. 530–533, 1908.

[10] N. Schunk and K. Petermann, “Noise Analysis of Injection-Locked Semiconductor Injection Lasers,” IEEE J. Quantum Electron., vol. 22, pp. 642-650, May 1986.

[11] D. Marcuse, “Computer Simulation of Laser Photon Fluctuations: Theory of Single-Cavity Laser,” IEEE J. Quantum Electron., vol. 20, pp.1139-1148, Oct. 1984.

[12] C. R. Mirasso, Pere Colet, and Priscila Garcia-Fernhdez, “Synchronization of Chaotic Semiconductor Lasers: Application to Encoded Communications,” IEEE Photonics Technology letters, vol. 8, pp. 299-301, Feb. 1996.

[13] K. M. Cuomo and A.V. Oppenheim, “Circuit implementation of synchronized chaos with applications to communications,” Phys. Rev. Lett., vol.71, pp. 65–68, 1993.

[14] L. Kocarev and U. Parlitz, “General Approach for Chaotic Synchronization with Applications to Communication,” Phys. Rev. Lett., vol.74, pp. 5028–5031, 1995.

[15] V. Ahlers, U. Parlitz, and W. Lauterborn, “hyperchaotic dynamics and synchronization of external-cavity semiconductor lasers,” Phys. Rev. E 58, pp.7208-7213, 1998.

[16] H. U. Voss, “Anticipating chaotic synchronization,” Phys. Rev. E 61, pp.5115–5119, 2000.

[17] J. Ohtsubo, “Chaos synchronization and chaotic signal masking in semiconductor lasers with optical feedback,” IEEE J. Quantum Electron., vol. 38, pp. 1141-1154, 2002.

[18] S. Peters-Flynn, P. S. Spencer, S. Sivaprakasam, I. Pierce and K.A. Shore, “Identification of the optimum time-delay for chaos synchronization regimes of semiconductor lasers,” IEEE J. Quantum Electron., vol. 42, pp. 427-434, 2006.

[19] E. C. Ifeachor and B. W. Jervis, Digital Signal Processing: A Practical Approach, 2nd edition, Prentice Hall, 2002.

Chapter 3

Optimised Operating Conditions of Analogue Message Modulation in Optical Chaos Communication

3.1 Introduction

The amount of information transmitted through communication systems is ever increasing. Internet banking and internet shopping require sensitive personal details transmission. To this end, public crypto systems based on software techniques have provided a platform for security. Improving the security of an encrypted message can be achieved by additional encoding at the physical hardware layer and, in particular, by using carriers generated chaos by components in the system. The chaotic output of a transmitter system is used as a carrier in which a message is encoded. The amplitude of the message is much smaller than the typical fluctuations of the chaotic carrier, so that it is very difficult to isolate the message. To decode the message, the transmitted signal is coupled to another chaotic system, the receiver, which is similar to the transmitter. The receiver synchronizes with the chaotic carrier itself; so that the message can be recovered by subtracting the receiver output from the transmitted signal [1-3]. The operation of optical chaotic communication systems is dependent upon the achievement of chaos synchronization. Pioneering work on the synchronization of two chaotic systems was reported by Cuomo and Oppenheim [4] who showed that systems displaying Lorenz chaos can be used to effect message transmission in a chaos communication system. In such schemes the message (M) is typically added to the chaotic laser emission (C) so that the output from the transmitter laser is M+C. Through the achievement of chaos synchronization the receiver laser output is C. The tendency of the receiver laser to synchronize only to the chaos and not the message is termed Chaos Pass Filtering (CPF) [5]. CPF enables message extraction. By subtracting the receiver output from that of the transmitter the message is recovered: symbolically we have (M+C) – C = M as in fig.1.3.

Colet and Roy first numerically demonstrated the possibility of hiding and recovering binary bit sequence at 100kbps using synchronization of chaos in two solid-state lasers [6]. In their scheme a message was encoded in the chaotic output of transmitter laser, and it was transmitted to the receiver laser using an optical fibre. The receiver laser was assumed to operate under similar conditions as the transmitter laser. Since then several schemes have been proposed for the exploitation of synchronized chaos in order to achieve secure communications using lasers [7-12]. For optical chaos communication, semiconductor lasers offer many advantages being both widely available and also being easily driven into chaos, for example by the use of external cavity feedback [13-17]. In 1999 Sivaprakasam and Shore were the first to demonstrate experimentally synchronization [18] and in 2000 message encoding and decoding [12] using chaotic external cavity semiconductor lasers. Work on synchronization [16] identified an optimum coupling strength requirement between transmitter and receiver laser to achieve good quality robust synchronisation.

The practical utility of a chaotic carrier in high-bit rate optical communications has been established using several chaotic laser diode transmitter-receiver configurations including a field trial over an installed optical fibre network [19]. The key physical requirement for effecting message extraction using such a system is the achievement of high-quality chaos synchronization between the transmitter laser (TL) and receiver laser (RL). In turn, that synchronization is reliant on the selection of a well-matched pair of laser diodes for the TL and RL.

In external cavity semiconductor laser systems it has been demonstrated that the receiver laser synchronizes with the chaos produced in the transmitter but that the masked message amplitude is much reduced in the receiver compared with that in the transmitter [20, 21]. The chaos pass filtering exhibited by synchronized laser diodes is frequency dependent [5, 17]: The closer the message frequency is to the relaxation oscillation frequency, the worse is the filtering of the message in the receiver laser. This property is expected to be highly important for the practical implementation of chaotic synchronized lasers in secure communication systems.

Laser operating conditions for high quality synchronization and high quality of signal to noise ratio (SNR) message extraction have been shown experimentally to be different

[22]. The aim in this chapter to identify ideal operating conditions wherein chaos synchronization and maximum SNR are achieved simultaneously performing numerical analysis on a semiconductor laser-based optical chaos communications system.

3.2 Numerical Model

The well-known Lang-Kobayashi model [18, 19] is use to identify ideal operating conditions for optimized chaos synchronization and message extraction. In this chapter the study is based on the analogue message modulation. The schematic diagram and the rate equations are discussed in chapter 2.

3.3 TL and RL Output Power and Synchronization

Simulations are performed on the Lang-Kobayashi model using the parameter values in table 3.1. The time series of the output powers of the TL and the RL are plotted in fig.3.1. The black solid line represents the TL output intensity and the red solid line represents the RL output intensity.

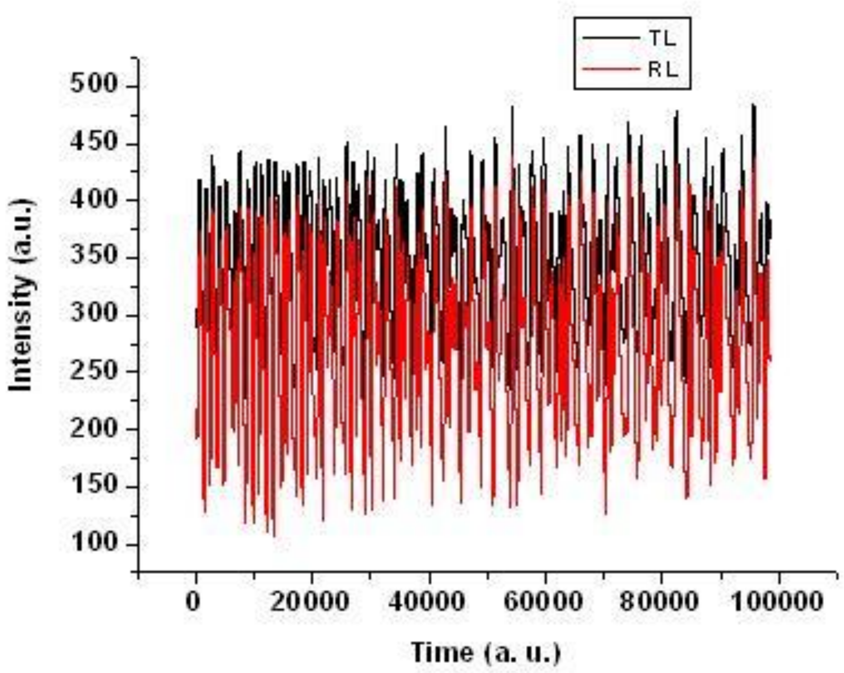

Fig.3.1. TL (black) and RL (red) chaotic output intensity versus Time.

Table: 3. 1

Parameter	Symbol	Values
Transmitter laser bias current	I_{TL}	25mA
Line width enhancement factor	α	5
Carrier lifetime	τ_N	2ns
Photon lifetime	τ_P	2ps
Transmitter laser external cavity round-trip time	τ_{ex}	1ns
Linear gain coefficient	g	$1.5\text{x}10^{-8}$ ps^{-1}
Gain saturation coefficient	ε	$5\text{x}10^{-7}$
Carrier number at transparency	N_0	$1.5\text{x}10^{8}$
Wavelength	λ	1551nm
Master laser feedback rate	κ_m	$10ns^{-1}$
Wavelength change of RL w.r.t. current	$d\lambda_{RL}/dI$	0.0142(nm/mA)

The TL output intensity at a given time versus the RL output intensity at the same time is plotted to demonstrate the synchronization between TL and RL. In fig.3.2 X-axis is TL output intensity and Y-axis is RL output intensity. The synchronization diagram is approximately synchronized and having the 45^0 slope of the synchronization line plot.

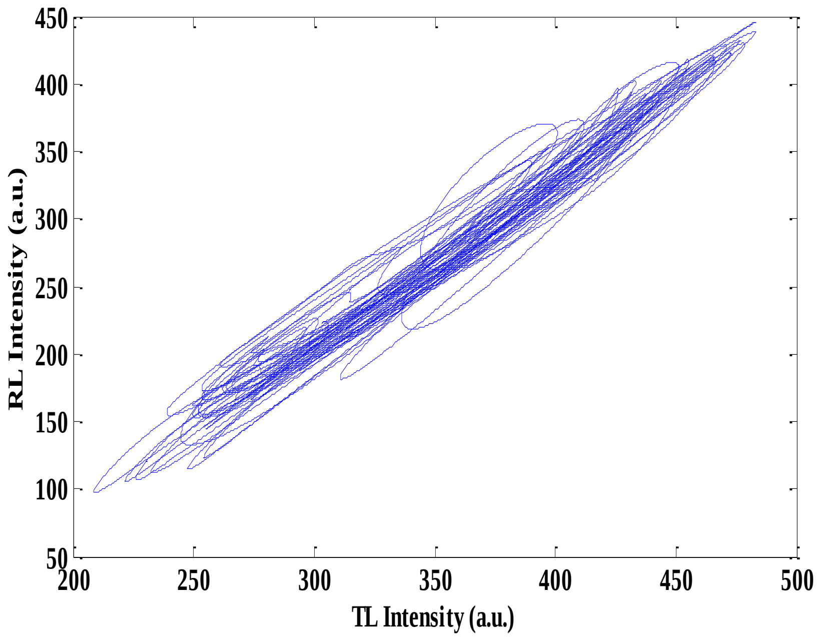

Fig.3.2. RL intensity vs. TL intensity.

The synchronization quality C(τ) between the TL and the RL was calculated using the cross correlation from equation2.19. The cross correlation function is discussed in chapter 2 section 2.7.1. C(τ) is calculated for a broad range of τ 1ns to 1ns. C(τ) vs. τ is plotted in fig.3.3.

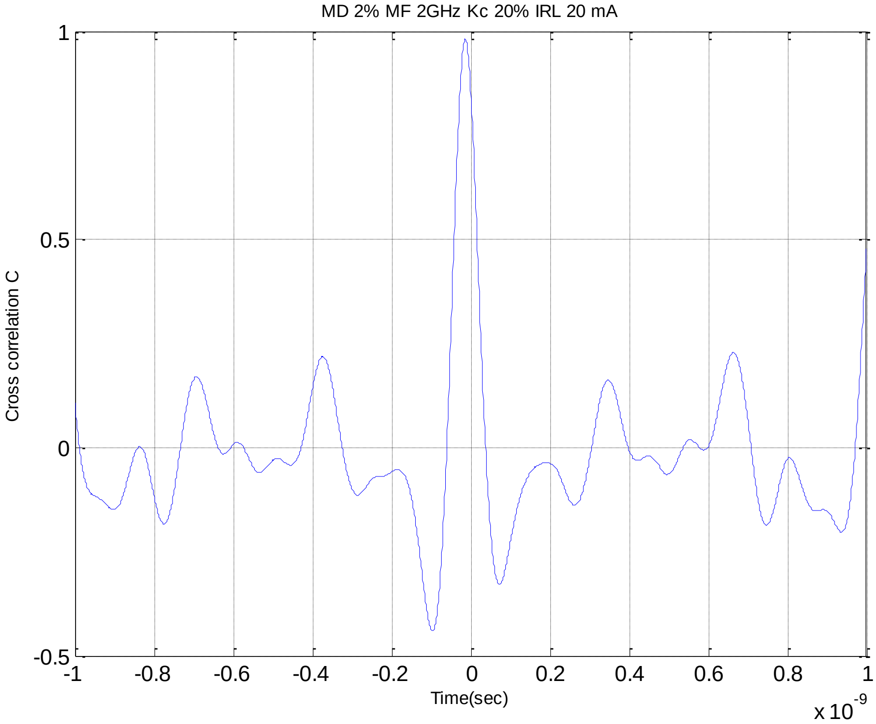

Fig.3.3. Cross correlation between TL and RL vs. time shift.

3.4 Signal to Noise Ratio of Extracted Message

Signal to noise ratio (SNR) is used to calculate the quality of extracted message. The signal to noise ration calculation is discussed in chapter 2 section 2.9.

In fig. 3.4 the SNR vs. the RL bias current is plotted. The modulation frequency of the signal is 2GHz. Modulation depth of signal is 4%. Coupling strength from TL to RL is 20%. Black solid line represents the SNR of extracted message and the red solid line represents the SNR of RL signal output. It is observed that the SNR of extracted message is higher than the RL output signal. This implies that the RL is only synchronizes to the chaotic noise of the TL.

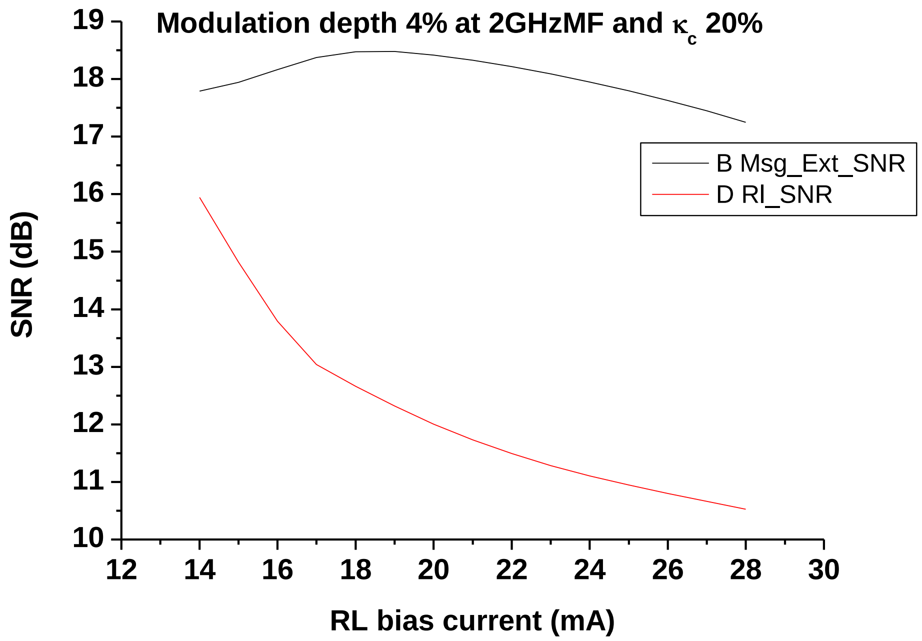

Fig. 3.4. SNR vs. RL Bias current. Black solid line represent SNR of extracted message and red represent RL NSR at modulation depth 4% and modulation frequency 2GHz.

3.5 Results

Fig.3.5 shows the results of calculations of the cross correlation between the transmitter and the receiver lasers and the SNR_{msg} of the extracted message as a function of the RL bias current. The figure was obtained for a modulation frequency of 2GHz, TL-RL coupling strength of 20% and TL signal modulation depth of 2%. It can be seen that the best synchronization - at a RL bias current of 17.8mA- does not coincide with the best message extraction – at a RL current of 18.1mA. This mismatch has been found over a wide range of signal modulation depths and TL-RL coupling rates and was observed experimentally in [22] for low values of the RL bias current the correlation coefficient is relatively small.

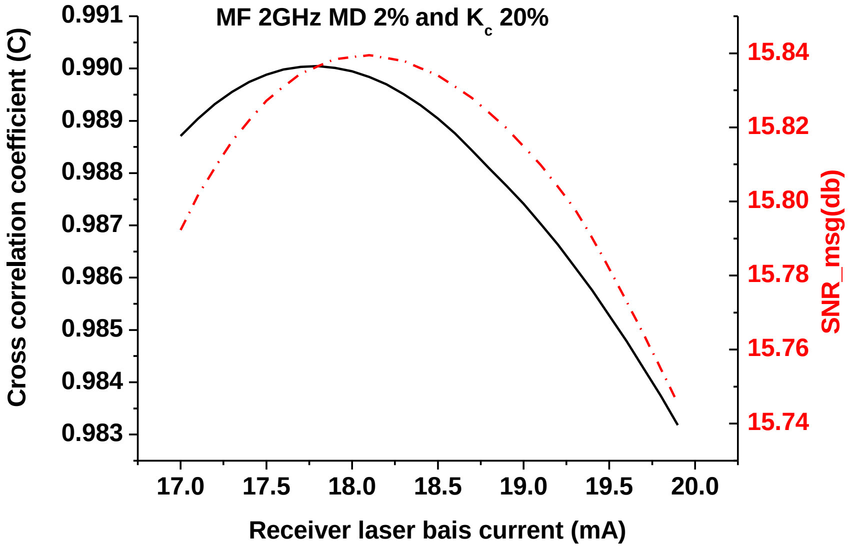

Fig.3.5. Black solid line represents the cross correlation as function of the RL bias current. Red dashed line represents the SNR as function of the RL bias current. Modulation depth is 2%, modulation frequency is 2GHz and coupling strength from TL to RL K_c is 20%.

As the RL bias current is increased the combined effect of the electrical injection and the light from the TL brings the RL operating point nearer to that of the TL. At a RL bias current of 17.8mA the TL and RL operating points are most alike, and the corresponding correlation coefficient is highest.

Further increases to the RL bias current beyond the optimum value increase the degree of mismatch between the TL and RL operating points, with a corresponding reduction in cross correlation coefficient.

When the TL bias current is reduced to 20mA, the RL bias current for optimum cross correlation condition also reduces, from 17.8mA to 17mA. If the RL current were not reduced at the same time then the combined effect of the RL bias current and the light injected from the TL would raise the operating point of the RL above that of the TL, with a corresponding reduction in the similarity between TL and RL signals accompanied by a reduction in cross correlation coefficient.

For good message extraction good synchronization is needed, so at low values of RL bias current the cross correlation coefficient is relatively small, hence the signal to noise ratio of extracted message is relatively small. As the bias current of RL is increased cross correlation coefficient is increased, at the same time the signal to noise ratio of the extracted message increases as seen in fig.3.5. With Further increases to the RL bias current beyond the optimum value cross correlation coefficient, there is some range where the signal to noise ratio of extracted message continuously increases to a maximum value and then starts to reduce.

3.5.1 Operating Conditions

In this section results are presented which illustrate the consequences of exploring a wider set of operating conditions in search of an optimal condition. Attention is given to the impact of the message modulation depth, modulation frequency and TL-RL coupling strength. Here the result is simulated for two sets of coupling strength values. The result is plotted for each coupling strength value to the study of the different modulation frequency condition and modulation depth condition.

3.5.1.1 Operating Condition of Coupling Rate 20% From TL to RL at Modulation Frequency 1-5GHz

A convenient method for displaying a range of operating conditions is to use contour plots for cross correlation and SNR measurement as a function of two controllable parameters. In fig.3.6 values of the cross correlation coefficient are found in the RL bias current /message modulation depth phase space. The results shown are obtained for a 1 GHz modulation frequency and 20% coupling rate between the TL and RL. The cross correlation contour plot in fig.3.6 captures the cross correlation for RL bias currents in the range 14mA-28mA (at increments of 1mA) and for the values of modulation depth in the range 1%, 6%, 10% and 15%. Such ranges are well within experimentally accessible limits. In the fig.3.6 the darkest area (red in colour plot) represents the highest value (0.98) of cross correlation coefficient; other values of the correlation coefficient appear in the figure. It is seen from fig.3.6 that the highest cross correlation coefficients are obtained at lower values of the modulation depth and that as the modulation depth is increased the cross correlation coefficient decreases. The highest cross correlation coefficients are found in the area between 1% - 2.5% modulation depths at 16mA – 21mA RL bias current.

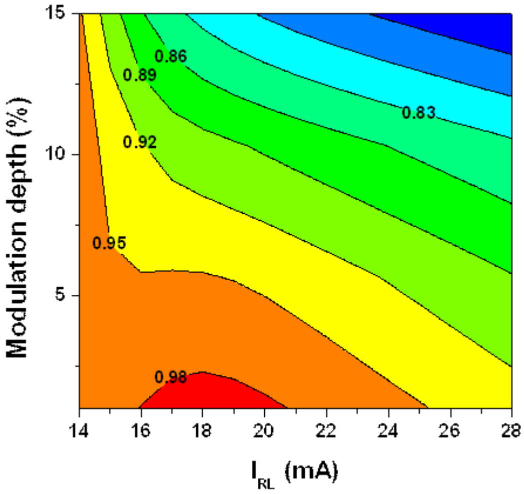

Fig.3.6. Cross correlation contour as a function of modulation depth and RL bias current at modulation frequency 1GHz and Kc 20%.

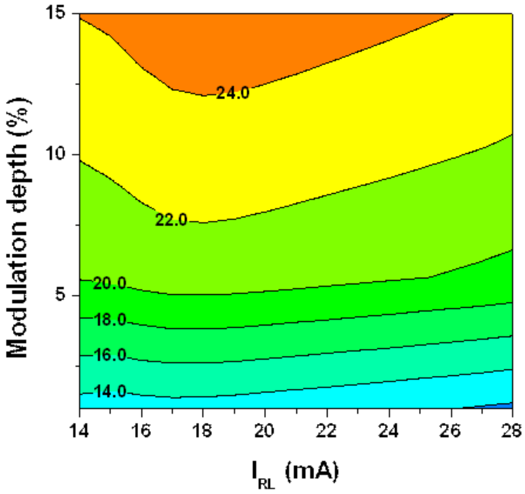

Fig. 3.7. SNR contour as a function of modulation depth and RL bias current at modulation frequency 1GHz and Kc 20%.

Fig.3.7 shows the dependence of the SNR of the extracted message again in the phase space of the RL bias current and the message modulation depth. As for fig.3.6 the results are obtained at a message modulation frequency of 1GHz and a 20% coupling rate between the TL and RL. The increments in the phase space parameters are the same as in fig.3.6. Analogously to fig.3.6 the contour coding associates the darkest area (red in colour plot) with the highest values of SNR. As can be anticipated, it is seen in fig.3.7 that the higher SNR is found at higher modulation depth and that the SNR decreases with decrease in modulation depth.

Fig.3.8&3.9 are contour plots of cross correlation and SNR respectively at 2GHz modulation frequency compared to fig. 3.6&3.7 at 1GHz modulation frequency. Coupling strength from TL to RL is 20%. It is observed that the cross correlation variation with respect to modulation depth and RL bias current is same as fig. 3.6. SNR variation with respect to modulation depth and RL bias current is same as fig. 3.7.

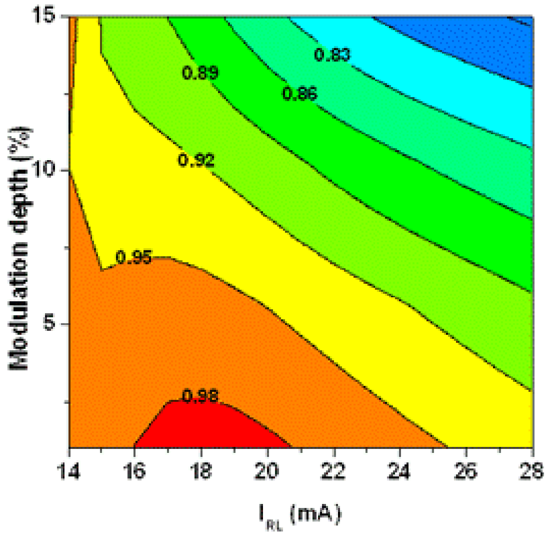

Fig. 3.8. Cross correlation contour as a function of modulation depth and RL bias current at modulation frequency 2GHz and Kc 20%.

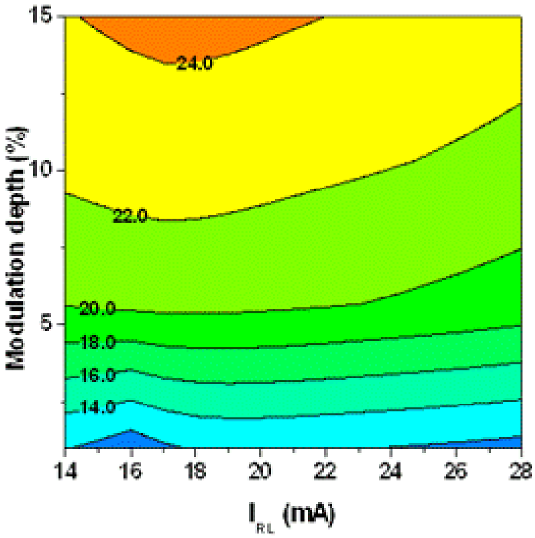

Fig. 3.9. SNR contour as a function of modulation depth and RL bias current at modulation frequency 2GHz and Kc 20%.

Fig. 3.10&3.11 are contour plots of cross correlation and SNR respectively at 3GHz modulation frequency compared to fig. 3.6&3.7 at 1GHz modulation frequency. The coupling strength from TL to RL is 20%. It is observed that the cross correlation variation with respect to modulation depth and RL bias current is same as fig. 3.6. SNR variation with respect to modulation depth and RL bias current is same as fig.3.7. It is observed in fig.3.10 that the area of good synchronization (red in colour) has increased compared to fig. 3.6. However the cross correlation variation with respect to modulation depth and RL bias current is same as fig. 3.6. The area of higher value of the SNR in fig. 3.11 has decreased compared to fig. 3.7. However the SNR variation with respect to modulation depth and RL bias current is same as fig. 3.7 increases and SNR decreases respectively for applied modulation depth and coupling strength as in fig. 3.6. It is observed that when the modulation frequency increases the cross correlation.

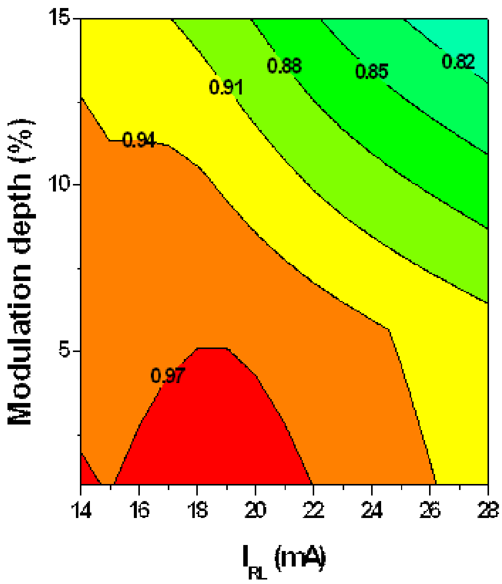

Fig. 3.10. Cross correlation contour as a function of modulation depth and RL bias current at modulation frequency 3GHz and Kc 20%.

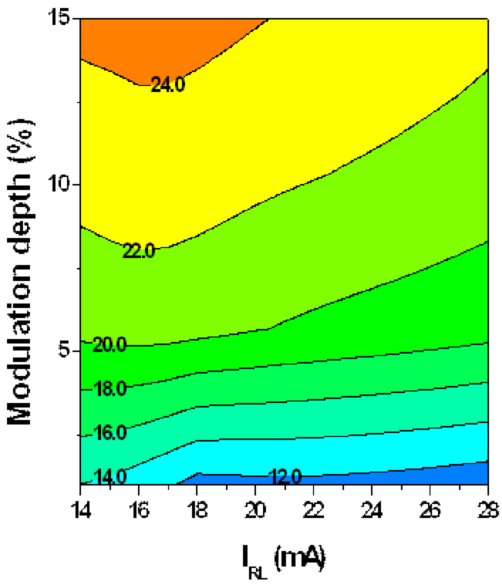

Fig. 3.11. SNR contour as a function of modulation depth and RL bias current at modulation frequency 3GHz and Kc 20%.

Fig. 3.12&3.14 are contour plots of cross correlation at modulation frequencies of 4GHz and 5GHz respectively. Other operating conditions are the same as fig. 3.6. It is observed that the good synchronization area (red in colour) is increased marginally compared to 1GHz modulation frequency. Fig.3.13&3.15 are contour plots of SNR at modulation frequencies 4GHz and 5GHz respectively. The conditions of modulation depth and coupling strength are same as fig. 3.7. It is observed that the higher SNR (red in colour) is deceased marginally compared to 1GHz modulation frequency.

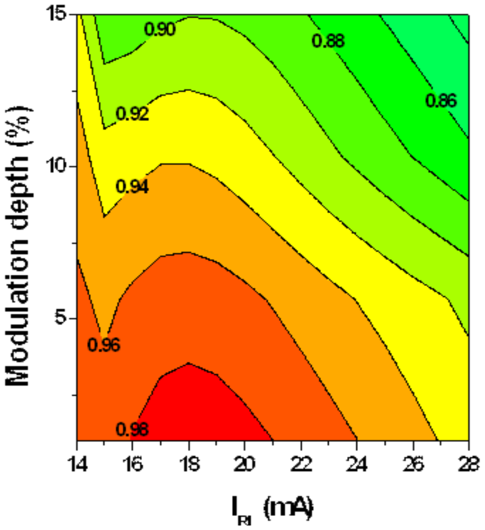

Fig.3.12. Cross correlation contour as a function of modulation depth and RL bias current at modulation frequency 4GHz and Kc 20%.

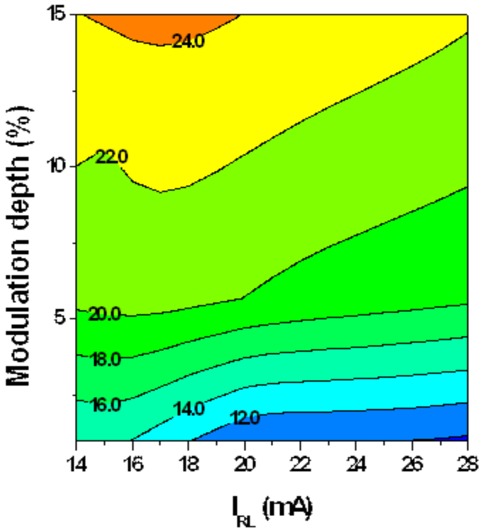

Fig.3.13. SNR contour as a function of modulation depth and RL bias current at modulation frequency 4GHz and Kc 20%.

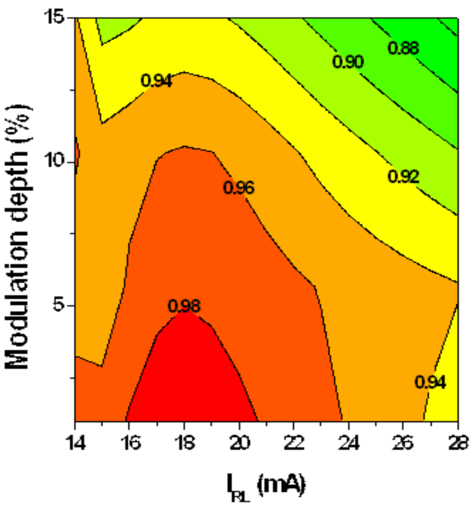

Fig.3.14. Cross correlation contour as a function of modulation depth and RL bias current at modulation frequency 5GHz and Kc 20%.

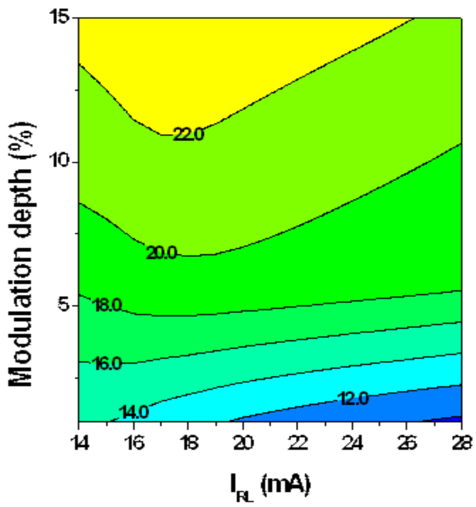

Fig.3.15. SNR contour as a function of modulation depth and RL bias current at modulation frequency 5GHz and Kc 20%.

It is observed that there is a lack of coincidence between the regimes of highest quality synchronization and maximum SNR from the above cross correlation and the SNR contour plots. Cross correlation increases with increases the modulation frequency whereas the SNR is decreasing with increases the modulation frequency. It may be expected that the regimes of maximum achievable cross correlation and maximum attainable SNR should have similar operating condition.

3.5.1.2 Operating Condition of Coupling Rate 40% from TL to RL at Modulation Frequency 1-5GHz

The coupling strength between the TL and the RL is an important parameter which affects the synchronization and SNR in an optical chaos communication system. It was numerically verified that strong coupling from TL to RL can enhance the modulation bandwidth of injection-locked semiconductor lasers [23]. In this section coupling strength from TL to RL increases to 40%.

Fig. 3.16 is contour plot of cross correlation at 1GHz modulation frequency and 40% coupling rate from TL to RL. It is observed that the cross correlation decreases (0.97) compared to fig.3.6 (0.98).

Fig.3.17 is contour plot of SNR at 1GHz modulation frequency and 40% coupling rate from TL to RL. It is observed that the SNR increases (26dB) compared to fig.3.7 (24dB). Hence cross correlation decreases and SNR increases with increased coupling strength from TL to RL.

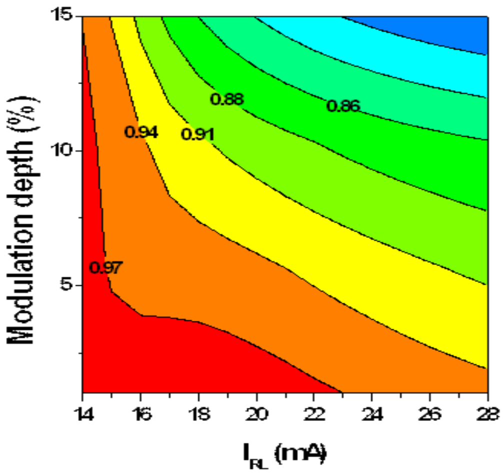

Fig.3.16. Cross correlation contour as a function of modulation depth and RL bias current at modulation frequency 1GHz and Kc 40%.

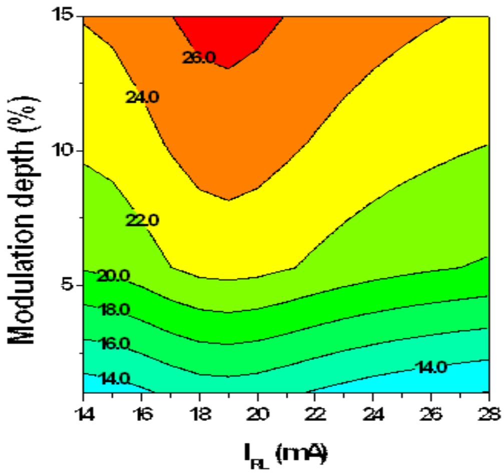

Fig.3.17. SNR contour as a function of modulation depth and RL bias current at modulation frequency 1GHz and Kc 40%.

Fig.3.18&3.19 are contour plots of cross correlation and SNR respectively at 2GHz modulation frequency and are compared with fig.3.16&3.17 for the case of 1GHz modulation frequency. It is observed that in fig.3.18 the cross correlation variation with respect to modulation depth and RL bias current is same as fig.3.16. SNR variation in the fig.3.19 with respect to modulation depth and RL bias current is same as fig.3.17.

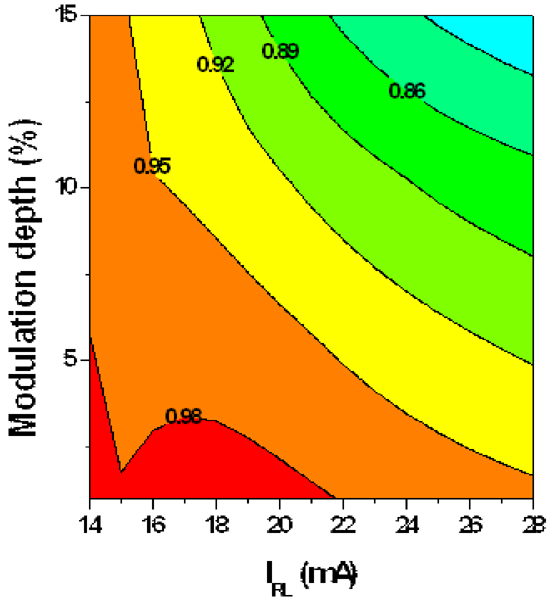

Fig.3.18. Cross correlation contour as a function of modulation depth and RL bias current at modulation frequency 2GHz and Kc 40%.

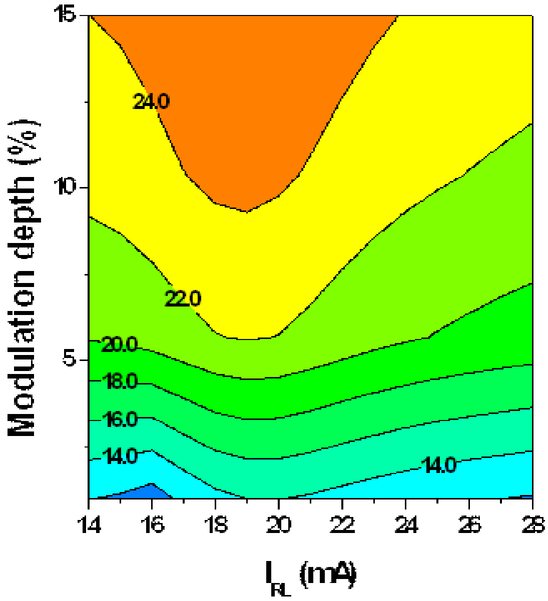

Fig.3.19. SNR contour as a function of modulation depth and RL bias current at modulation frequency 2GHz and Kc 40%.

Fig.3.20&3.21 are contour plots of cross correlation and SNR respectively at 3GHz modulation frequency compared to fig.3.16&3.17 at 1GHz modulation frequency. Coupling strength from TL to RL is 40%. It is observed that the cross correlation variation with respect to modulation depth and RL bias current is same as fig.3.16. SNR variation with respect to modulation depth and RL bias current is same as fig.3.17. It is observed in fig.3.20 that the area of good synchronization (red in colour) has increased compared to fig.3.16. However the cross correlation variation with respect to modulation depth and RL bias current is same as fig.3.16. The area of higher value (red in colour) of the SNR in fig.3.21 has decreased compared to fig.3.17. However the SNR variation with respect to modulation depth and RL bias current is same as fig.3.17.

It is observed that when the modulation frequency increases cross correlation increases and SNR decreases respectively for applied modulation depth and coupling strength as in fig.3.16 – 3.21.

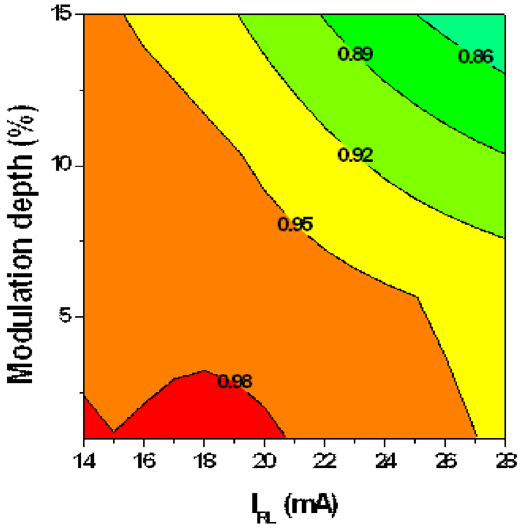

Fig.3.20. Cross correlation contour as a function of modulation depth and RL bias current at modulation frequency 3GHz and Kc 40%.

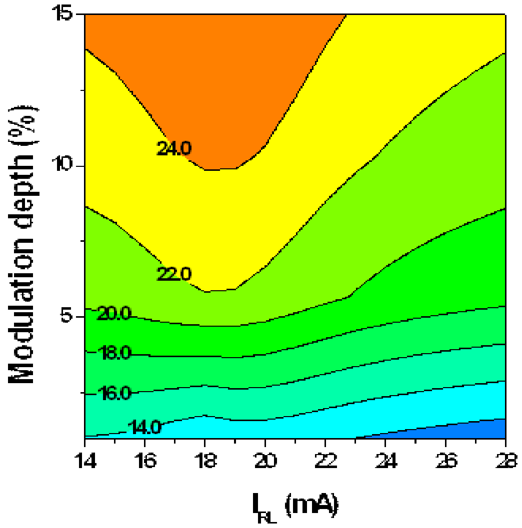

Fig.3.21. SNR contour as a function of modulation depth and RL bias current at modulation frequency 3GHz and Kc 40%.

Fig.3.22&3.24 are contour plots of cross correlation at modulation frequency 4GHz and 5GHz respectively. Other operating conditions are same as fig.3.16. It is observed that the good synchronization area (red in colour) is increased marginally compared to 1GHz modulation frequency. Fig.3.23&3.25 are contour plots of SNR at modulation frequency 4GHz and 5GHz respectively. Conditions of modulation depth and coupling strength are same as fig.3.17. It is observed that the higher SNR (red in colour) is deceased marginally compared to 1GHz modulation frequency.

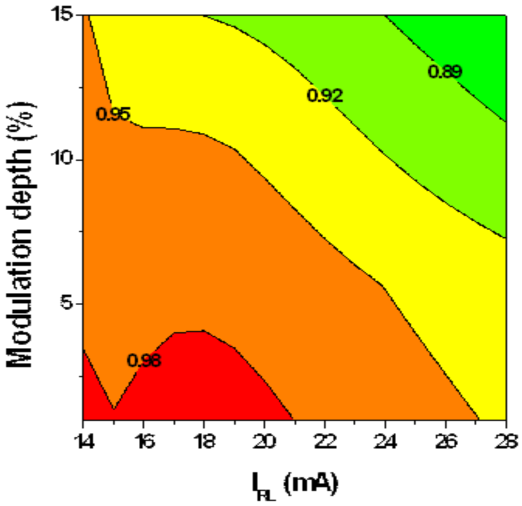

Fig.3.22. Cross correlation contour as a function of modulation depth and RL bias current at modulation frequency 4GHz and Kc 40%.

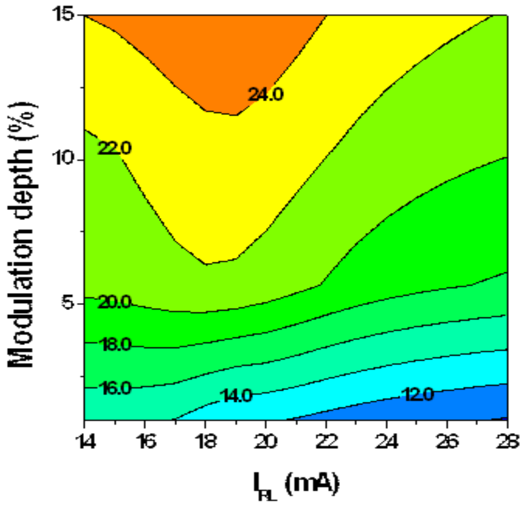

Fig.3.23. SNR contour as a function of modulation depth and RL bias current at modulation frequency 4GHz and Kc 40%.

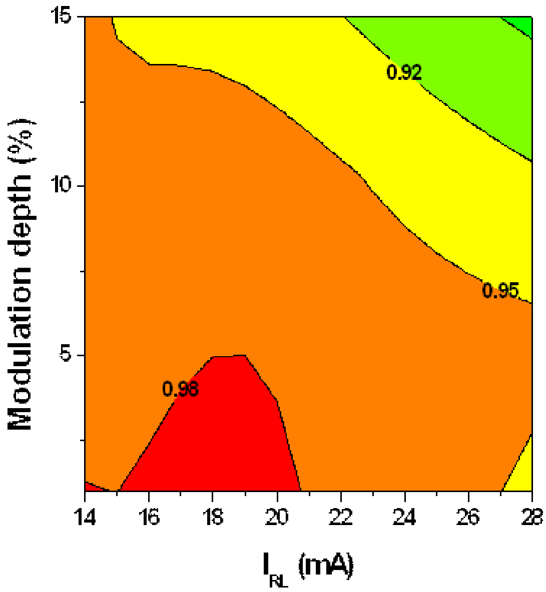

Fig.3.24. Cross correlation contour as a function of modulation depth and RL bias current at modulation frequency 5GHz and Kc 40%.

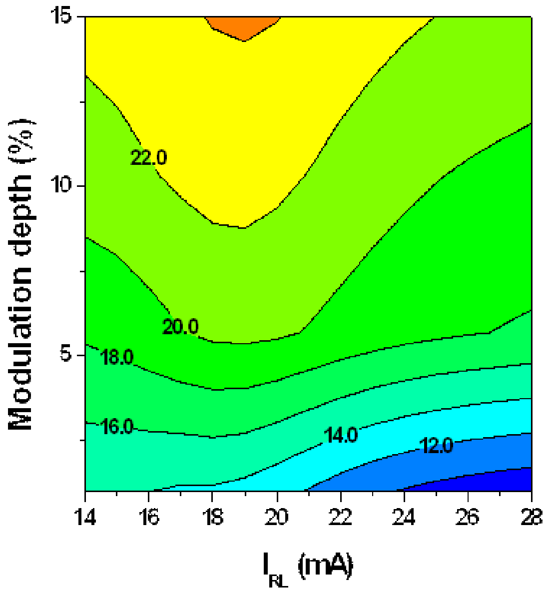

Fig.3.25. SNR contour as a function of modulation depth and RL bias current at modulation frequency 5GHz and Kc 40%.

It is observed from the above figures, the cross correlation decreases as coupling rate increases from the TL to RL and SNR increases as coupling rate increases from the TL to RL.

Cross correlation increases with increases the modulation frequency whereas the SNR is decreasing with increases the modulation frequency.

It is also absorbed from the above figures; the regimes of maximum cross correlation do not coincide with maximum SNR. This is accordance with experimental observations [22].

It may be expected that the regimes of maximum achievable cross correlation and maximum attainable SNR should have similar operating condition without compromising the security of message transmission.

3.5.2 Maximum Cross Correlation and Maximum SNR

Fig.3.26 & 3.27 shows the maximum cross correlation and maximum SNR variation as function of modulation depth at coupling strength from TL to RL 20% and 40% respectively. Vertical left and right axes represent the cross correlation and the SNR respectively. The black solid line represents cross correlation. The red dashed line represents SNR.

It is observed from fig.3.26 & 3.27 that the maximum cross correlation coincidence with the maximum SNR near a 3% modulation depth.

Having executed this study of wider parameter dependences of the quality of chaos synchronization and message extraction efficiency attention is now given to the key results of the present work: the identification of operating regimes where the highest quality synchronization and most efficient message extraction can be simultaneously achieved.

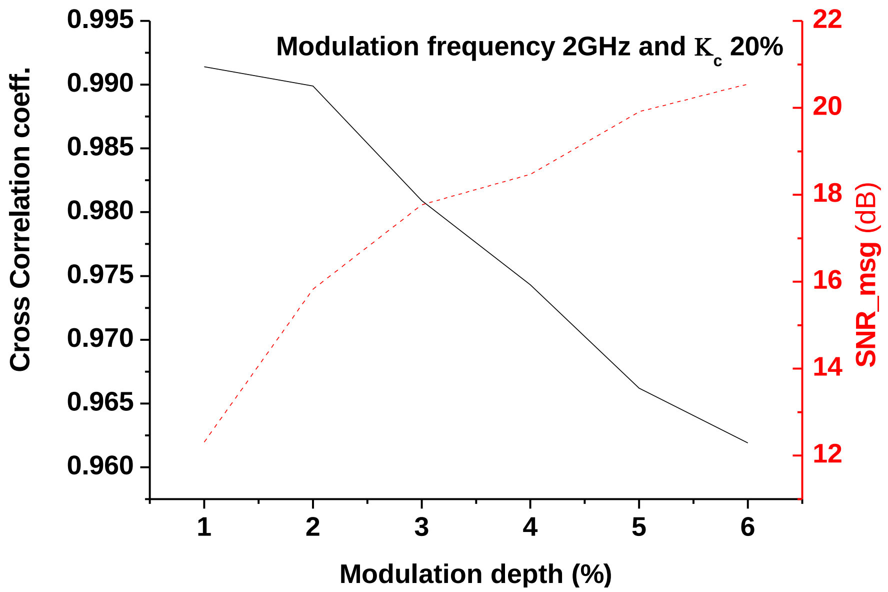

Fig.3.26 Cross correlation vs. modulation depth on left side of the graph. SNR vs. modulation depth on right side of the graph. The black solid line represents cross correlation and the red dashed line represents SNR. Modulation frequency is 2GHz and coupling strength Kc is 20%.

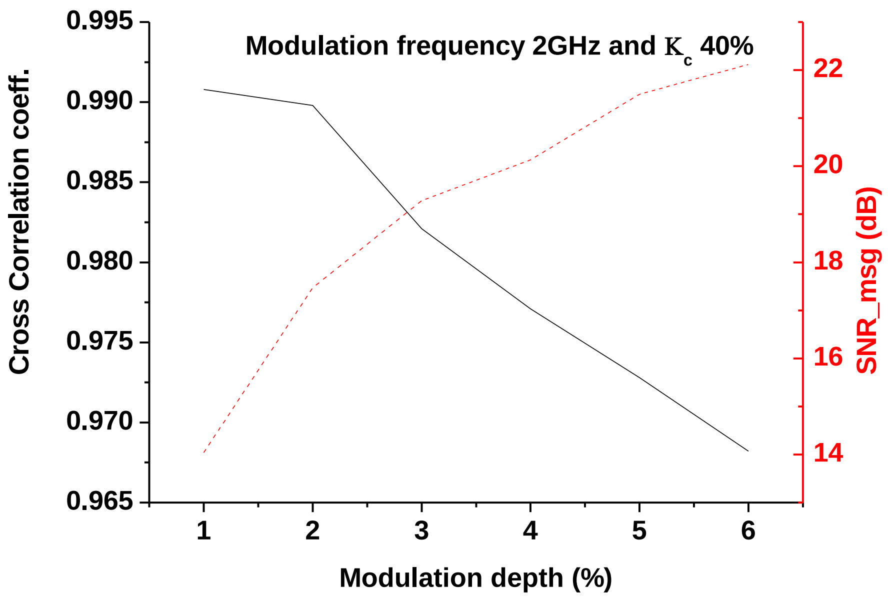

Fig.3.27 Cross correlation vs. modulation depth on left side of the graph. SNR vs. modulation depth on right side of the graph. The black solid line represents cross correlation and the red dashed line represents SNR. Modulation frequency is 2GHz and coupling strength Kc is 40%.

3.5.3 Identification of Optimised Operating Conditions

It has been shown in the specific cases treated in the preceding section that the RL bias current for maximum cross correlation coefficient does not coincide with that for maximum SNR of the extracted message. This is in accordance with experimental observations [22] and was found generally to be the case in a wide range of simulations. From the view point of practical deployment of optical chaos communications this has serious implications since the discrepancy between the conditions for optimized chaos synchronization and those for highest SNR in message extraction will require that in situ adjustments of laser operating conditions are required in order to maximize SNR and hence minimize error rates in transmission.

The focus is here to identify operating conditions wherein chaos synchronization and maximum SNR are achieved simultaneously. It is appreciated that laser parameters modulation depth, modulation frequency and coupling rate TL/RL may be adjusted in order to improve the quality of chaos synchronization properties. For definiteness attention is concentrated here on the role of the receiver laser bias current in determining the synchronization properties. In this case the specific objective of this work is to locate the receiver laser bias current which enables coincident achievement of optimized chaos synchronization and maximum SNR in message extraction.

The explicit means for revealing such an optimized operating regime is to determine the conditions which provide the minimum difference between the RL bias current for the maximum SNR which is denoted by I_{SNR_max} and the RL bias current for the best synchronization which is denoted by I_{C_max}. The key parameter for these calculations is the difference between these two currents $\Delta I = I_{SNR\_max} - I_{C\_max}$. Clearly the ideal is to locate operating conditions for which that current difference is zero. Having undertaken extensive simulations near ideal operating conditions have been identified. From an experimental view point the most accessible parameters for adjusting the operating conditions are the coupling rates between the TL and the RL and the message modulation depth. It is noted that there are practical limitations to the ranges of these parameters which may be considered. In relation to the coupling rates it is considered that values in the range 20 % to 40 % are appropriate. In respect of the modulation depth one observes that there is a trade-off between message extraction and security of transmission: if the modulation depth is too small then message extraction may be inhibited; if the modulation depth is too large then the expected security of transmission may be compromised. Following such considerations one identifies a range of usable modulation depths between 1% and 10%.

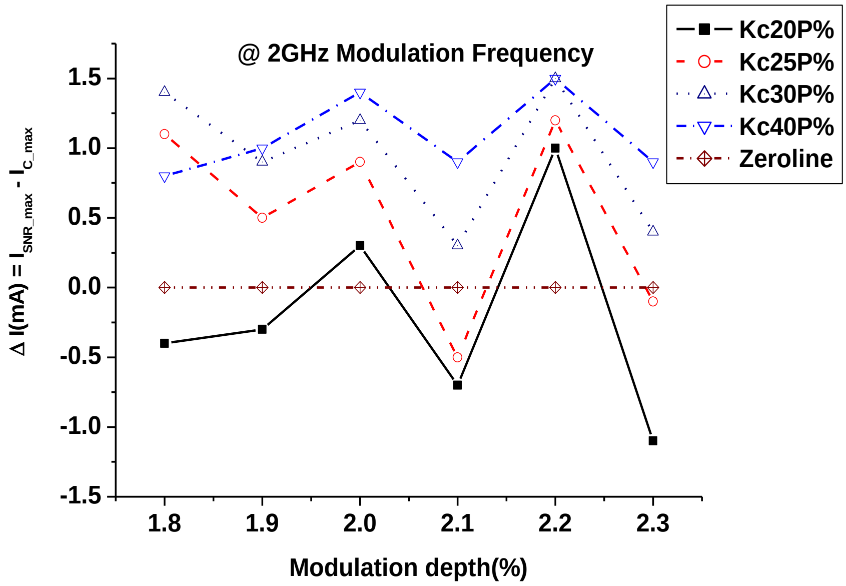

Fig.3.28. Modulation depth versus ΔI is plotted at 2GHz modulation frequency. Coupling rate from TL to RL are 20%, 25%, 30% and 40% indicated by different symbols.

In fig.3.28, for example, the current difference, ΔI, is shown as a function of the modulation depth for a modulation frequency 2GHz and for different TL to RL coupling rates. It is seen that for coupling rates of 40% and 30% ΔI remains non-zero over the range of modulation depths explored. For coupling rates of 25% and 20% there are indications that a zero ΔI can be obtained albeit within comparatively narrow ranges of modulation depth. The dependence of ΔI on the modulation depth shows a similar pattern for all coupling rates but with the higher coupling rates exhibiting the greatest deviation from the ideal.

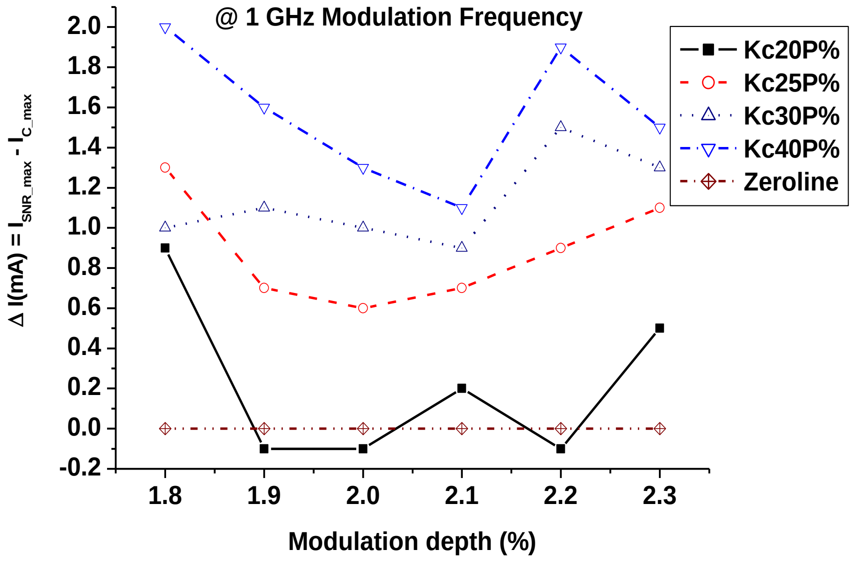

Fig.3.29. Current difference ΔI versus modulation depth is plotted at 1GHz modulation frequency. Coupling rate from TL to RL are 20%, 25%, 30% and 40% as different line.

Fig.3.29 shows calculations performed with essentially the same conditions as in figure 28 except that the modulation frequency here is 1 GHz. The dependence of ΔI on the modulation depth exhibits similar patterns for different TL to RL coupling rates as those of fig.3.28. However the highly significant case is that of a 20% coupling rate. Here ΔI attains values very close to zero over a relatively wide range of modulation depths between 1.9 % and 2.2 %. Such regions of reduced sensitivity to change in modulation depth are likely to be practically useful.

In comparison, Fig.3.28 & 3.29 confirms that ideal operating conditions can be accessed wherein high-quality chaos synchronization coincides with maximum SNR in message extraction. Specifically in the case of 1GHz modulation frequency and a 20% TL to RL coupling rate ideal operating conditions are found for a modulation depth of order 2%.

3.6 Conclusion

With a view to practical deployment of laser-diode based optical chaos communications, synchronization of the transmitter laser and receiver laser is necessary. Good synchronization enables high quality message recovery. Synchronization depends on the operating conditions of the transmitter laser and receiver laser. An optimal operating condition is identified where high-quality chaos synchronization coincides with maximum message extraction efficiency. Attention has been focused on using the receiver laser bias current as an experimentally adjustable physical quantity to achieve the defined ideal operating conditions. In this way it has been found that an optimal configuration for 1GHz modulation frequency may utilize a 2% modulation depth and 20% TL-RL coupling rate. Having established a methodology for identifying the defined optimal operating conditions the opportunity is now opened to apply the approach more generally. Specific interest will be focused on applying the approach to digital message transmission with a view to identifying optimal Bit-Error-Rates. In that context the modulation frequency dependences of the performance will have particular relevance. Such explorations are discussed in next chapter. In addition it is intended to effect an experimental verification of the optimal operating characteristics identified in the present work.

References

[1] L. M. Pecora and T. L. Carroll, “Synchronization in chaotic systems”, Phys. Rev. Lett., vol. 64, pp. 821–823, 1990.

[2] L. M. Pecora and T. L. Carroll, “Driving systems with chaotic signals”, Phys. Rev. A, vol. 44, pp. 2374–2383, 1991.

[3] K. A. Shore and D. T. Wright, “Improved synchronization algorithm for chaotic communications systems”, Electron. Lett., vol. 30, pp. 1203–1204, 1994.

[4] K. M. Cuomo and A.V. Oppenheim, “Circuit implementation of synchronized chaos with applications to communications”, Phys. Rev. Lett. Vol.71, pp. 65–68 ,1993

[5] J. Paul, M. W. Lee, and K. A. Shore, “Effect of chaos pass filtering on message decoding quality using chaotic external-cavity laser diodes”, Opt. Lett., vol. 29, pp. 2497–2499, Nov. 2004.

[6] P. Colet and R. Roy, “digital communication with synchronized chaotic lasers”, Opt. Lett. 19 2056-2058 (1994)

[7] Y. Liu, P.C. De Oliveira, M.B. Danailov, and J.R. Rios Leite, “Chaotic and periodic passive Q switching in coupled CO2 lasers with a saturable absorber”, Phys. Rev. A, vol. 50, pp. 3464, 1994.

[8] P. Colet and R. Roy, "Digital communication with synchronized chaotic lasers", Opt. Lett., vol.19, pp. 2056, 1994.

[9] G. D. VanWiggeren and R. Roy, "Communication with Chaotic Lasers", Science, vol. 279, pp. 1200, 1998.

[10] G. D. VanWiggeren and R. Roy, "Optical Communication with Chaotic Waveforms", Phys. Rev. Lett., vol. 81, pp. 3547, 1998.

[11] S. Sivaprakasam and K. A. Shore, "Signal masking for chaotic optical communication using external-cavity diode lasers", Opt. Lett., vol. 24, pp. 1200–1202, 1999.

[12] S. Sivaprakasam and K. A. Shore, "Message encoding and decoding using chaotic external-cavity diode lasers", IEEE J. Quantum Electron., vol. 36, pp. 35–39, Jan. 2000

[13] R. Lang and K. Kobayashi, "External optical feedback effects on semiconductor injection laser properties", IEEE J. Quantum Electron., vol. 16, pp 347-355 1980.

[14] S. Sivaprakasam and K. A. Shore, "Demonstration of optical synchronization of Chaotic external laser diode", Opt. Lett. Vol. 24, pp.466-468,1999.

[15] D. M. Kane and K. A. Shore (Editors), Unlocking Dynamical Diversity: Optical Feedback Effects on Semiconductor Lasers, John Willey & Sons, Ltd, 2005.

[16] I. Fisher, Y. Liu, and P. Davis, "Synchronization of chaotic semiconductor laser dynamics on subnanosecond time scales and its potential for chaos communication", Phys. Rev. A, vol. 62, art. no. 011801(R), 2000.

[17] A. Uchida, Y. Liu, and P. Davis, "Characteristics of chaotic masking in synchronized semiconductor lasers", IEEE J. Quantum Electron., vol. 39, pp. 963–970, Aug. 2003.

[18] S. Sivaprakasam and K. A. Shore, "Demonstration of optical synchronization of Chaotic external laser diode", Opt. Lett. Vol. 24, pp.466-468,1999.

[19] A. Argyris, D. Syvridis, L. Larger, V. Annovazzi-Lodi, P. Colet, I. Fischer, J. García- Ojalvo, C. R. Mirasso, L. Pesquera, and K. A. Shore, "Chaos-based communications at high bit rates using commercial fibre-optic links", Nature, vol. 438, pp. 343–346, Nov. 2005.

[20] A. Murakami and K. A. Shore, "Chaos-pass filtering in injection-locked semiconductor lasers", Phys. Rev. A, vol. 72, art. no. 053810, 2005.

[21] Y. Li, Y. Wang, and A. Wang, “Message filtering characteristics of semiconductor laser as receiver in optical chaos communication”, Optics Commun., vol. 281, pp. 2656–2662, 2008.

[22] Y. Hong, M. W. Lee, and K. A. Shore, “Optimised Message Extraction in Laser Diode Based Optical Chaos Communications”, IEEE J. Quantum Electron., vol.46 pp.253-257, 2010.

[23] A. Murakami, “Synchronization of chaos due to linear response in optically driven semiconductor lasers”, Phys. Rev. E 65, 056617, 2002.

Chapter 4

Digital Optical Chaos Communications

4.1 Introduction

In the previous chapter transmission of an analogue message using a chaotic optical carrier was discussed. In this chapter the transmission of digital information is explored. As in the previous chapter use will be made of a semiconductor laser subject to external optical feedback to provide the requisite optical chaos. Utilization of digital data in relation to a chaotic optical signal is important in several applications e.g. physical random bit generation [1, 2], optical chaos logic gate realization for optical chaos computing [3] and neural network analysis [4, 5].

In the specific context of optical chaos communications a digital message may be encoded onto the chaotic optical carrier output of the transmitter laser (TL) by e.g. the direct current modulation of the drive current of the TL. For the external cavity semiconductor laser of interest here the Lang-Kobayashi model [6, 7] is used for the complex slowly varying amplitude of the electrical field and minority carriers inside the cavity of the TL. The model used includes spontaneous emission noise [8].

The practical utility of a chaotic carrier in high-bit rate optical communications has been established using several chaotic laser diode transmitter-receiver configurations including a field trial over an installed optical fibre network [9]. The key physical requirement for effecting message extraction using such a system is the achievement of high-quality chaos synchronization between the transmitter laser (TL) and receiver laser (RL). In turn, that synchronization is reliant on the selection of a well-matched pair of laser diodes for the TL and RL [10].

Laser operating conditions for high quality synchronization and high quality of signal to noise ratio message extraction have been shown experimentally to be different [10]. In this chapter a numerical analysis of a semiconductor laser-based digital message transmitter system is performed with a view to identifying optimal operating conditions where the highest-quality synchronization and most efficient message extraction can be obtained simultaneously.

Schematic diagrams of the optical chaos communication system and an introduction to the well-known Lang-Kobayashi model have been provided in chapter 2 section 2.2.

4.2 Numerical Model Including Langevin Noise

In practical semiconductor laser systems noise is inevitably present and may have a significant impact on the performance of the laser. To realistically model the behaviour of a practical laser system, it is therefore important to include the effects of noise [8, 11-13]. Work on the description of noise sources in semiconductor lasers can be traced to the earliest days of semiconductor laser development [14-16]. Emerging from that work a widely accepted approach is to describe the effects of noise in terms of so-called Langevin noise. The key properties of Langevin noise sources have been discussed in Chapter 2 section 2.6. Briefly it is recalled that Langevin noises are random noise induced by spontaneous emission. Mathematically the main feature of Langevin noise sources is that they are added directly to the dynamical equations of interest. The well-known Lang-Kobayashi model [7, 8] including Langevin noise is used to simulate the behaviour of digital modulation in an optical chaos communications system have been discussed in Chapter 2 section 2.5.

4.3 Digital Modulation and Chaotic Carrier Generation

In order to exemplify the operation of a digital optical communications scheme, a binary random bit sequence (BRBS) message is impressed via the transmitter laser drive current which thereby comprises a DC component and a message (modulating) component:

$$I_{TL} = I_{dc}(1 + h(BRBS)) \tag{4.1}$$

The BRBS is uniformly distributed random bit sequence of zeros and ones. Here I_{dc} is the bias current of the transmitter laser and h is the modulation depth.

4.4 Cross Correlation

As in the chapter 2, the synchronization quality between the outputs of the TL and RL is calculated using cross correlation function as discussed in section 2.7.1.

4.5 Bit Error Rate

A Key measure of the transmission performance of a digital communication system is the Bit Error Rate (BER). BER is the number of errors in the received bits divided by the total number of transmitted bits.

$$BER = \frac{Number\ of\ bit\ errors}{Total\ number\ of\ bits} \tag{4.2}$$

Optical communication systems are normally designed with the objective of achieving BER of less than 10^{-12}. It is noted that, in practice, error correction schemes may be used to ensure that the desired BER is obtained. No consideration is given here to the utilisation of any such error correction protocols.

To quantify the message decoding efficiency at the receiver, calculations are performed to determine the BER of the extracted message. For better message extraction high cross correlation is required between the TL and the RL [17]. In this work it is assumed that there is no propagation time delay between the TL and the RL i.e. a back-to-back configuration is considered (chapter 2 section 2.3.2). To find the BER in the decoded message, message extraction is performed in two steps. In the first step, as explained in chapter 2 section 2.7.1, the time delay between TL intensity and RL intensity at maximum correlation is calculated. In the second step the RL time series output intensities are shifted by the time delay of maximum correlation. Then message extraction is performed by subtracting the RL intensity from the TL intensity. An intensity threshold I_{th} value for decision making on the received bit is defined. If the output intensity is greater than $I_{th;}$ then the bit will be considered as a 1 otherwise the bit will be taken to be a 0.

I_{max} is defined as maximum intensity value of the extracted message and I_{min} is minimum intensity value of extracted message. Then:

$$I_{th} = I_{min} + (\text{difference between } I_{max} \text{ and } I_{min})/2 \tag{4.3}$$

$$\text{i.e. } I_{th} = I_{min} + (I_{max} - I_{min})/2 \tag{4.4}$$

4.6 Results

In the calculations reported here, attention has been given to the impact of variations of the DC bias current of the receiver laser on (i) the synchronization quality, quantified as the maximum value of the cross-correlation function; and (ii) the BER of the extracted message. For the present calculations, it is assumed that the DC bias current of the transmitter laser is fixed at $2I_{th}$ (25mA) and wavelength of the TL is 1550nm. A binary random bit sequence message signal of modulation depth h (1% - 3%) and message transmission rate f (1 GB/s-3 GB/s) is transmitted. The RL bias current is varied from 17mA to 20mA. Parameter values used in the numerical simulations are listed in table 4.1. The corresponding relaxation oscillation frequency (ROF) of the diode laser is calculated to be 4 GHz.

Table 4.1: Simulation parameters

Parameter	Symbol	Value
Transmitter laser bias current	I_{TL}	25mA
Line width enhancement factor	α	5
Spontaneous emission factor	β	$1.1\text{x}10^{-9}$ps
Carrier lifetime	τ_N	2ns
Photon lifetime	τ_P	2ps
Transmitter laser external cavity round-trip time	τ_{ext}	1ns
Linear gain coefficient	g	$1.5\text{x}10^{-8}\text{ps}^{-1}$
Gain saturation coefficient	ε	$5\text{x}10^{-7}$
Carrier number at transparency	N_0	$1.5\text{x}10^{8}$
Transmitter laser Wavelength	λ_{TL}	1550nm
Transmitter laser feedback rate	K_m	10ns^{-1}
Wavelength change of RL w.r.t. current	$d\lambda_{RL}/dI$	0.0142 (nm/mA)

4.6.1 Correlation and BER

In this section results are presented which illustrate the consequences of exploring a wide set of operating conditions to find the desired optimal operating condition. Laser operating conditions for high quality synchronization and high quality of signal to noise ratio message extraction have been shown experimentally to be different [10]. With a view to ensuring both efficient message recovery and the security of the message transmission, specific attention is given to the impact of the message modulation depth.
A convenient method for displaying a range of operating conditions is to use contour plots for the cross correlation and BER as a function of two controllable parameters.

In fig.4.1, using a 20 % coupling rate K_C between the TL and RL, values of the cross correlation coefficient are found in the RL bias current - message modulation depth, h, phase space. In fig.4.1 the red area represents the highest obtained value (0.98) of the cross correlation coefficient. It is seen that the highest cross correlation coefficients are obtained at lower values of the modulation depth and that as the modulation depth is increased the cross correlation coefficient decreases. The highest cross correlation coefficients are found in the area between 1.5%-1.7% modulation depths at 17.5mA – 18.75mA RL bias current.

Fig.4.2 shows the dependence of the BER of the extracted message again in the phase space of the RL bias current and the message modulation depth. Analogously to fig.4.1 the contour coding associates the red area with the lowest values of BER. As can be anticipated, it is seen in fig.4.2 that the lower BER is found at higher modulation depth and that the BER increases with decrease in modulation depth.

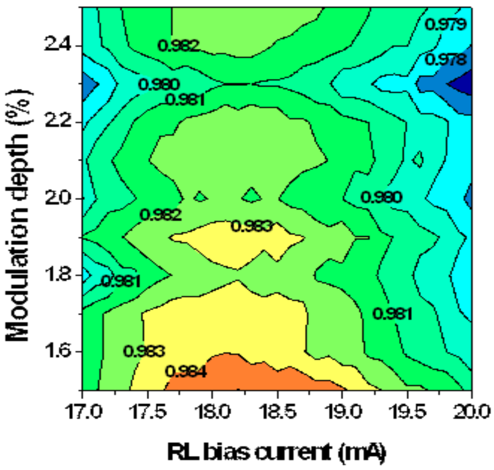

Fig.4.1. Cross correlation contour as a function of modulation depth and RL bias current at message transmission rate 3 GB/s and K_c 20%.

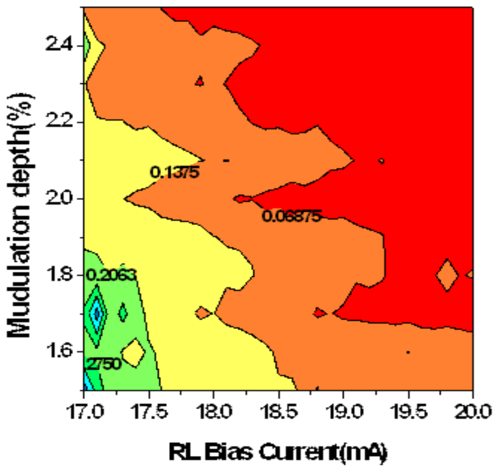

Fig.4.2. BER contour as a function of modulation depth h, and RL bias current at message transmission rate 3 GB/s and K_c 20%.

Even a cursory glance at fig.4.1 & 4.2 shows clearly the lack of coincidence between regimes of highest quality synchronization and minimum BER in message extraction. The same phenomenon is observed in the case of analogue modulation discussed in chapter 3.

Fig.4.3&4.4 are contour plots of cross correlation and BER respectively at 2 GB/s modulation frequency. The coupling strength from TL to RL is maintained at 20%. It is observed that the cross correlation variation with respect to modulation depth and RL bias current is increased with respect to the case in fig.4.1 (where the transmission rate was 3 GB/s). In fig.4.4 the BER is improved as modulation depth increases and message transmission rate decreases in comparison with the case in fig.4.2 at same RL bias current and coupling strength.

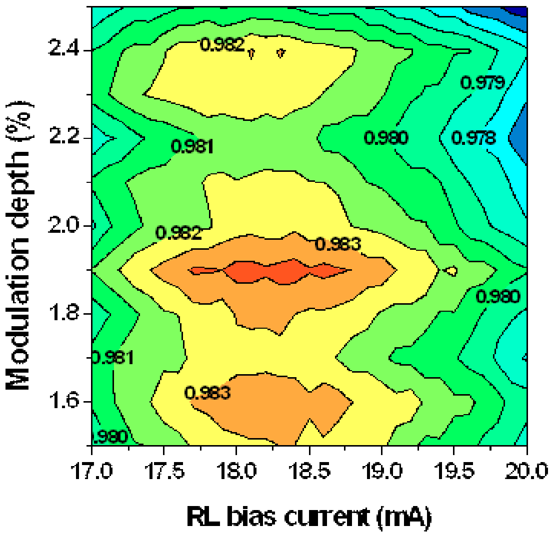

Fig.4.3. Cross correlation contour as a function of modulation depth and RL bias current at message transmission rate 2 GB/s and K_c 20%.

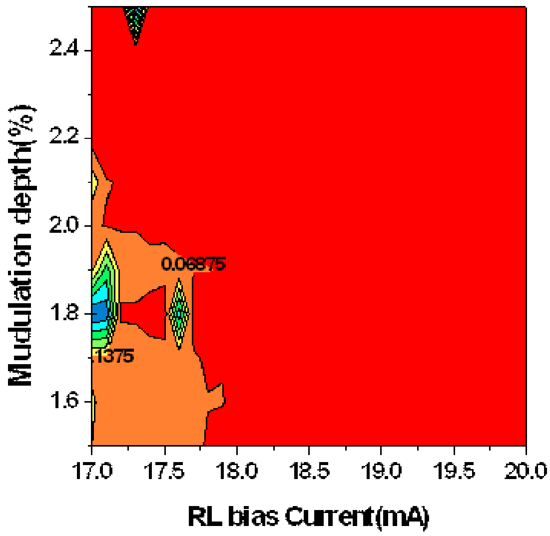

Fig.4.4. BER contour as a function of modulation depth h, and RL bias current at message transmission rate 2 GB/s and K_c 20%.

In fig.4.5&4.6 the message transmission rate is 1GB/s and the coupling strength K_c is 20%. It is observed that the area of higher values cross correlation coefficient decreases in fig.4.5. In fig.4.6 the lower values of BER have a larger area.

When the modulation depth increases, the parameter mismatch between the TL and the RL increases. Hence the cross correlation coefficient between the TL and the RL is reduced. When the modulation depth increases the message strength is higher so the BER improves under these conditions. It is observed from fig.1-6 that as the modulation depth increases the cross correlation coefficient decreases and the BER improve.

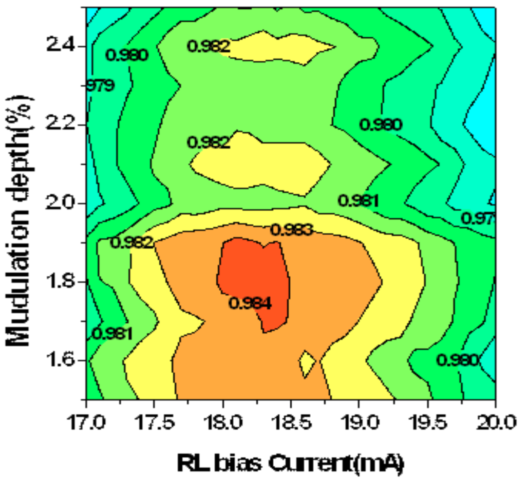

Fig.4.5. Cross correlation contour as a function of modulation depth and RL bias current at message transmission rate 1 GB/s and K_c 20%.

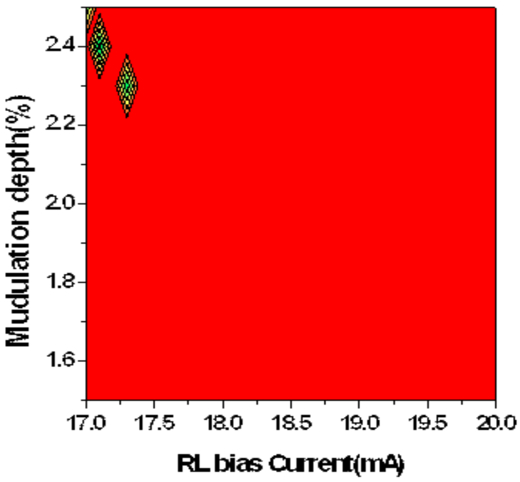

Fig.4.6. BER contour as a function of modulation depth h, and RL bias current at message transmission rate 1 GB/s and K_c 20%.

4.6.2 Effect of Varying the Message Transmission Rate at a Fixed Modulation Depth

The message transmission rate is an important characteristic of a digital optical chaos communication system. In this section the effect of varying the transmission rate at fixed modulation depth is discussed. The cross correlation contour is drawn as function of data transmission rate and RL bias current. In fig.4.7 the cross correlation is 0.985 at bias current 17.75mA to 19mA at lower modulation frequencies. The clear expectation is that BER should increase with modulation frequency or equivalently transmission rate. This is confirmed in fig.4.8 that the BER is lower at lower modulation frequency for the whole range of bias current.

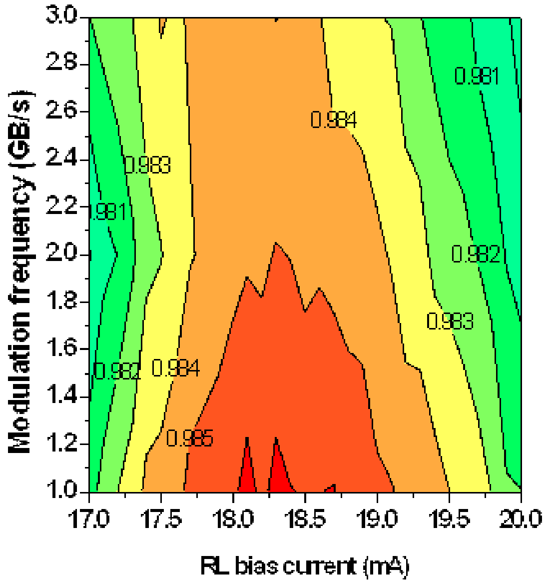

Fig.4.7. Cross correlation contour as a function of data transmission rata and RL bias current at message modulation depth 1% and K_c 20%.

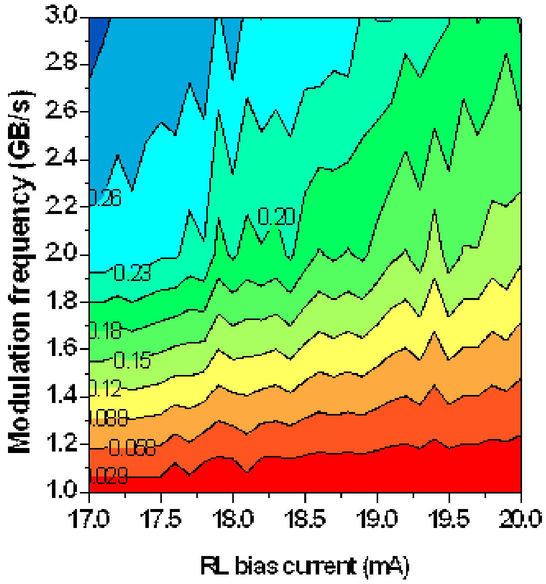

Fig.4.8. BER contour as a function of data transmission rata, and RL bias current at message modulation depth 1% and K_c 20%.

4.6.3 Optimal Operating Condition

From the viewpoint of practical use of optical chaos communications any discrepancies between the conditions for optimized chaos synchronization and those for lowest BER in message extraction will require that in situ adjustments of laser operating conditions are performed in order to minimize error rates in transmission.

It is appreciated that several laser parameters may be adjusted in order to improve the quality of chaos synchronization properties. For definiteness, attention is concentrated here on the role of the receiver laser bias current in determining the synchronization properties. In this case the specific objective of this work is to locate the receiver laser bias current which enables coincident achievement of optimized chaos synchronization and minimum BER in message extraction.

The explicit means for revealing such an optimized operating regime is to determine the conditions which provide the minimum difference between the RL bias current for the minimum BER which is denoted by I_{BER_min} and the RL bias current for the highest cross-correlation in synchronization which is denoted by I_{C_max}. The key parameter for these calculation is the difference between these two currents $\Delta I = I_{BER\_min} - I_{C\_max}$. Clearly the ideal is to locate operating conditions for which that current difference is zero. Having undertaken extensive simulations close-to-ideal operating conditions have been identified. In respect of the modulation depth one observes that there is a trade-off between message extraction and security of transmission: if the modulation depth is too small then message extraction may be inhibited; if the modulation depth is too large then the expected security of transmission may be compromised.

In fig.4.9, the current difference, ΔI, is shown as a function of the modulation depth for message transmission rate 1, 2 and 3 GB/s at 25% TL to RL coupling rates. It is seen in fig.4.9 that the operating condition line at 1, 2 and 3 GB/s departs from the ideal line. At these conditions it is difficult to find optimal operating condition.

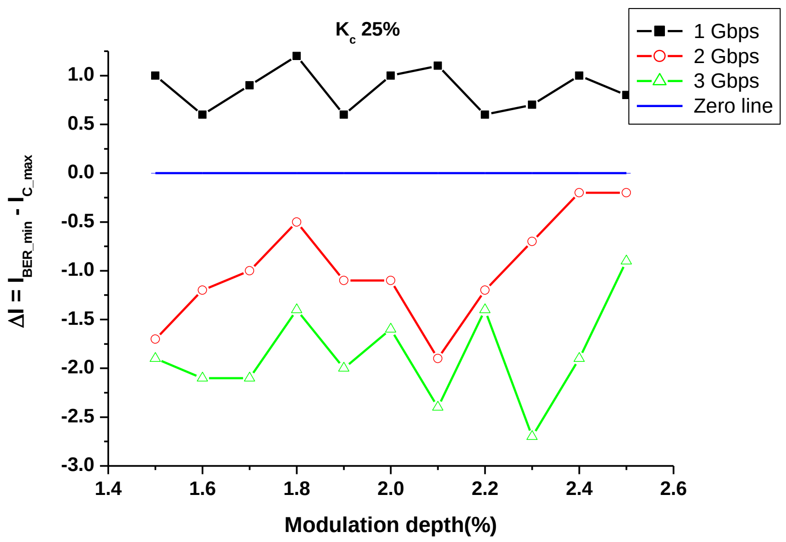

Fig.4.9. Current difference, ΔI, versus modulation depth, h, for 25% coupling rate from TL to RL.

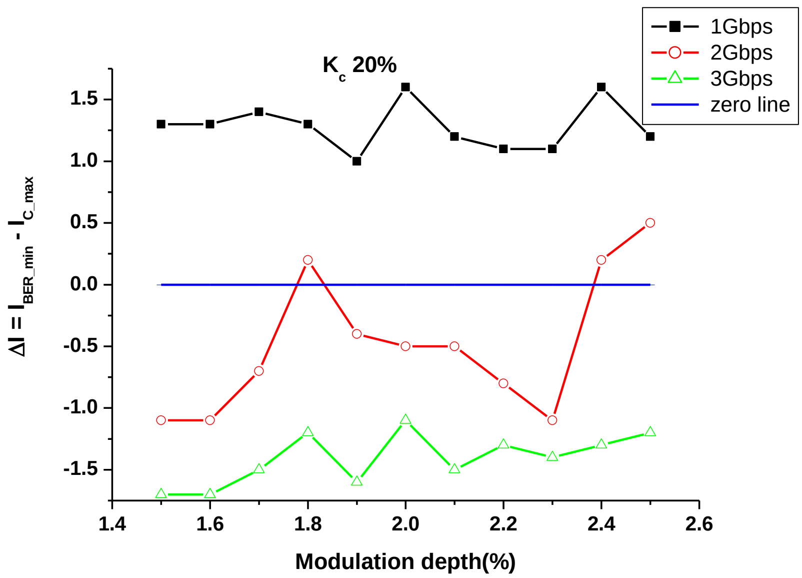

Fig.4.10. Current difference, ΔI, versus modulation depth, h, for 20% coupling rate from TL to RL.

In fig.4.10, the current difference, ΔI, is shown as a function of the modulation depth for message transmission rate 1, 2 and 3 GB/s at 20% TL to RL coupling rates. It is seen in fig.4.10 at 2 GB/s (red line circular symbols) transmission rate the ΔI line approaches the ideal line, whereas at 1 GB/s (black line rectangular symbols) and 3 GB/s (green line triangle symbols) the ΔI departs from the ideal condition for coupling rates from TL to 20%. There are indications that a zero ΔI can be obtained albeit within a comparatively narrow range of modulation depths.

4.7 Conclusion

In this chapter the transmission of digital information is explored. Utilization of digital data in relation to a chaotic optical signal is important in several applications e.g. physical random bit generation, optical chaos logic gate realization for optical chaos computing and neural network analysis.

With a view of practical utility of a chaotic carrier in digital optical chaos communication system, optimal operating conditions have been identified. Attention has been focused on using the receiver laser bias current as an experimentally adjustable physical quantity to achieve the defined ideal operating conditions. Different conditions of message transmission rate, modulation depth and coupling rate have been simulated. In this way it has been found that an optimal configuration for 2 GB/s message transmission may utilize a 1.8% modulation depth and 20% TL-RL coupling rate.

References

[1] A. Uchida, K. Amano, M. Inoue, K. Hirano, S. Naito, H. Someya, I. Oowada , T. Kurashige, M. Shiki, S. Yoshimori, K. Yoshimura, and P. Davis, “Fast physical random bit generation with chaotic semiconductor lasers,” Nature Photon., vol. 2, pp. 728–732, Nov. 2008.

[2] I. Kanter, Y. Aviad, I. Reidler, E. Cohen, and M. Rosenbluh, “An optical ultrafast random bit generator,” Nature Photon., vol. 4, pp. 58–61, Dec. 2010.

[3] K. E. Chlouverakis and M. J. Adams, “Optoelectronic realisation of NOR logic gate using chaotic two-section lasers,” IEE Electronics Letters, vol.41, pp. 359–360, Mar. 2005.

[4] M. R. Guevara, L. Glass, M. C. Mackey, and A. Shrier, “Chaos in Neurobiology,” IEEE Transctions on Systems, Man, and Cybernetic, vol. 13, pp. 790-798, 1983.

[5] A. Babloyantz and C. Lourenco, “Brain Chaos and Computation,” International Journal of Neural Systems, vol. 7, pp. 461-471, 1996.

[6] R. Lang and K. Kobayashi, “External optical feedback effects on semiconductor injection laser properties,” IEEE J. Quantum Electron., vol.16, pp. 347-355, 1980

[7] D. M. Kane and K. A. Shore, “Unlocking Dynamical Diversity: Optical Feedback Effects on Semiconductor Lasers,” John Willey & Sons Ltd, England, 1st edition, 2005.

[8] L. N. Langley and K. A. Shore, “Intensity noise and linewidth characteristics of laser diodes with phase conjugate optical feedback,” IEE Proc.-Optoelectron., vol. 141, No. 2, April 1994.

[9] A. Argyris, D. Syvridis, L. Larger, V. Annovazzi-Lodi, P. Colet, I. Fischer, J. García-Ojalvo, C. R. Mirasso, L. Pesquera, and K. A. Shore,“Chaos-based communications at high bit rates using commercial fibre optic links,” Nature, vol. 438, pp. 343–346, Nov. 2005.

[10] Y. Hong, M. W. Lee, and K. A. Shore, “Optimised Message Extraction in Laser Diode Based Optical Chaos Communications,” IEEE J. Quantum Electron., vol.46 pp.253-257, 2010.

[11] C. R. Mirasso, P. Colet, and P. Garcia-Fernhdez, “Synchronization of Chaotic Semiconductor Lasers: Application to Encoded Communications,” IEEE Photonics Technology letters, vol. 8, no. 2, pp. 299 Feb. 1996.

[12] A. Sanchez-Diaz, C. R. Mirasso, P. Colet, and P. Garcia-Fernandez, “Encoded Gbit/s Digital Communications with Synchronized Chaotic Semiconductor Lasers,” IEEE J. Quantum Electron., vol. 35, no. 3, pp.292, March 1999.

[13] N. Schunk and K. Petermann, senior member, IEEE, “Noise Analysis of Injection-Locked Semiconductor Injection Lasers,” IEEE J. Quantum Electron., vol. 22, no. 5, pp642, May 1986.

[14] H. Haug, “Quantum-mechanical rate equation for semiconductor lasers,” Phys. Rev., vol. 184, pp. 338-348, Aug. 1969.

[15] H. Haug, "Quantum mechanical theory of fluctuations and relaxation in semiconductor lasers," Zeitschrift für Physik A Hadrons and Nuclei, vol.200, Issue 1, pp 57-68, 1967.

[16] B. Lax, “Semiconductor lasers,” Annals of the New York Academy of Sciences vol. 122, pp. 598–607, May 1965.

[17] J. Paul, M. W. Lee, and K. A. Shore, “Effect of chaos pass filtering on message decoding quality using chaotic external-cavity laser diodes,” Opt. Lett., vol. 29, pp. 2497–2499, Nov. 2004.

Chapter 5

Time-Delay Signature Concealment in an Optical Chaos Communications System

5.1 Introduction

In the previous chapters the optimal operating regime of modulation depth, modulation frequency and feedback strength is found for best synchronization and maximum message extraction efficiency in optical chaos communications systems. In this chapter, time delay signature concealment is examined as function of bias current and feedback strength, with a view to improving the security of message transmission.

Optical chaos generated in semiconductor lasers has potential for applications in high speed secure communications [1, 2]. Often, external feedback from an external mirror is used to drive semiconductor lasers into broadband chaos. The external feedback incorporates periodic temporal components related to the time delay (TD) associated with the external cavity formed between the laser and the external mirror. As a consequence, the resultant chaotic oscillations typically include recurrence features termed time delay signatures [3, 4]. The TD signatures may offer an eavesdropper the opportunity to extract a key parameter of the optical chaos system and hence may compromise the security of a chaos-based optical communications system [5, 6]. Thus in order to ensure the security of a chaos-based cryptosystem the elimination of TD signatures is a topic of some importance.

Rontani et al. have theoretically investigated TD identification by using autocorrelation and mutual information techniques [7, 8]. The feedback rate and the difference between the external cavity time delay and the relaxation oscillation period of the semiconductor laser were the key parameters of the study. Rontani et al. identified two conditions which could prevent an eavesdropper from accessing the TD. One condition was the use of a low optical feedback rate and also to ensure substantial separation between the external cavity TD and the period of relaxation oscillation. The other condition considered was of low feedback rate with the external cavity TD close to the period of relaxation oscillation. The TD concealment is observed in the external cavity feedback semiconductor laser system by choosing the precise parameters. Curiously, high dimensional chaos does not necessarily correspond to TD concealment [9]. As such, the study of the characteristics of the TD signature is of great interest for the determination of the security of optical chaos communication systems utilizing external cavity lasers. Time delay identification has been studied using statistical approaches [10-15], involving, for example autocorrelation function and delay information theory.

Time delay concealment in a master-slave configuration has been reported experimentally and numerically, where the slave laser is subject to master laser chaotic output injection [16]. Jia-Gui Wu et al. have studied the TD signature elimination in mutually delay-coupled semiconductor laser (MDC-SL) systems [17]. They experimentally observed TD signature eliminated signal in a MDC-SL system under specific condition of coupling strength and frequency detuning.

Amongst the variety of semiconductor lasers which are commercially available, vertical cavity surface emitting lasers (VCSELs) have particular attractions for many applications including optical chaos communications. Attractive features of VCSELs include single longitudinal mode operation, circular output beam, low threshold current and low cost [18-21]. A particular feature of VCSELs which are typically circular cross section is that the direction of the typical linearly polarization emission is not usually well-defined and may undergo switching between two orthogonal directions termed X and Y in this work. This is illustrated in fig.5.1. The rich polarization properties of the VCSELs motivate investigations of the effect of polarization rotation of optical feedback on the TD signature.

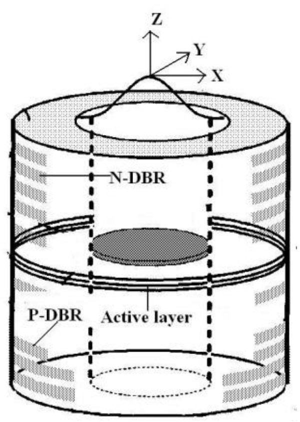

Fig. 5.1 Schematic structure of a VCSEL

S Xiang et.al [22] undertook a theoretical study of the effect of variable optical polarization- angle of feedback in VCSELs. They found that at low feedback strength the TD signature is concealed in the fully developed chaotic output of the VCSELs for all polarization-angles. While for moderate feedback strength they found that the TD signature is concealed at intermediate polarization-angles. However according to that study, for high feedback strength the TD signature is not concealed for any polarization-angle.

The basic motivation for the present work is to explore experimentally such theoretical predictions. As such, a scheme of optical feedback incorporating variation of the polarization-angle of optical feedback into VCSELs is used to find the appropriate conditions for TD concealment and thereby enhance the security of optical chaos communication systems.

5.2 Experimental Configuration

The experimental configuration of an external cavity VCSEL is shown schematically in fig.5.2. The VCSEL (AVAP-850SM VCSELTO46 w/MPD) has an operating wavelength of 850nm and a threshold current of 3.4mA. The VCSEL is driven with a low noise current source (Tektronix LDC202 200mA) and is temperature controlled within 0.01^{o} C. The beam-splitter (BS) sends a part of the laser output into the external cavity [7, 8, 23] and the remainder to the detection arm. An external-mirror (M, reflectivity 99.9 %) is used to return part of the laser beam to the VCSEL thereby defining the external cavity. An optical attenuator (VA) is placed in the external cavity to control the optical feedback strength. A quarter wave plate (QWP) is used to rotate the plane of polarization of the VCSEL emission. When a QWP is double passed due to mirror reflection, it acts as a half wave plate. Here the QWP is placed in external cavity of the VCSEL. Different polarization direction of optical feedback can be achieved by rotating the QWP through an angle θ_P. Due to the mirror reflection of laser beam the rotation of the plane of polarization of the light θ_{PR} is thereby changed by $2\theta_P$. The photodetecter (New Focus 1554-B-50, 12-GHz bandwidth) is used to detect the output of the VCSEL and recorded using a digital oscilloscope (Lecroy 7404, 4 GHz). In these measurements, the sampling rate of the oscilloscope is set to 10 GS/s and samples are recorded over a period of 10μs.

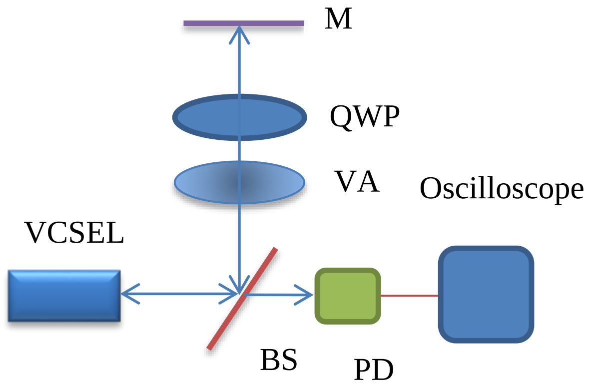

Fig.5.2. Schematic of variable optical polarization-angle feedback external cavity VCSEL system. BS: beam splitter; VA: variable attenuator; QWP: quarter wave plate; M: mirror; PD: photodetector.

5.3 Time Delay Signature Analysis Methods

The auto-correlation function (ACF) is used to retrieve the TD signature from the chaotic intensity of the VCSEL. The ACF is defined as follows [7, 8].

$$C_T(\Delta t) = \frac{<[I_T(t+\Delta t) - <I_T(t+\Delta t)>][I_T(t) - <I_T(t)>]>}{\sqrt{<[I_T(t+\Delta t) - <I_T(t+\Delta t)>]^2><[I_T(t) - <I_T(t)>]^2}} \tag{5.1}$$

Here I_T is output intensity of the VCSEL. < >denotes time average. Δt is the time interval between two intensities of a time series chaotic output of the VCSEL.

Based on calculated C_T values; the amplitude of the peak is calculated as the peak signal to mean ratio (PSMR). The PSMR is denoted as C_P and defined in eq.(5.2). The measured TD τ may not be located exactly at the true TD τ_d [21]. If the measured TD τ value is located in the interval $V_{(\tau d)} = (\tau_d - \tau_d \times r, \tau_d + \tau_d \times r)$; the TD will be consider retrieved. Here r the time mismatch coefficient is taken to be 5%.

$$C_P = \frac{max|C_T(\Delta t)|_{\Delta t \in V(\tau_d)}}{<|C_T(\Delta t)|>} \tag{5.2}$$

Where $<|C_T(\Delta t)|>$ is the averaged auto-correlation value of the chaotic output intensities of the VCSEL at different time delays. Clearly a higher value of

$max|C_T(\Delta t)|_{\Delta t \in V(\tau_d)}$ with a lower average value $< |C_T(\Delta t)| >$ results in a higher value of C_P.

In this work another time delay estimator is also used, which was introduced by Bandt and Pompe namely the information theory-based permutation entropy (PE) which is a measure of the complexity of the time series [24]. This method of time delay estimation is simple and fast.

In this method, a set U of the measured output intensities of the VCSEL is composed of N elements I_j where j = 1….N. Suppose the data is collected at a data rate of 10GS/s thus there is a typical time, T_S, between samples of 0.1ns. As such, of order 10^5 samples are obtained in each measurement. From these samples, subsets S_q containing M values of the measured intensities are defined in following way: for a defined time interval $T>T_S$, the elements of S_q are $I_{q - (m-1)T}$. where m = 1,…,M. In this way the first element of S_q is I_q and the remaining elements are the subsequent intensities at fixed time interval T. The intensities in each subset will conform with some pattern of relative magnitudes (for example, I_1 in a 4 element subset, $I_1 \geq I_2 \geq I_4 \geq I_3$). For a subset of M elements there will be M factorial (M!) such patterns. The association of a given subset with a given pattern is recorded. For the samples obtained with a time interval T, N-(M-1)XT/T_S subset of M element can be formed. Conformity of each such subset with the intensity patterns is recorded. In this way the probability P that a given pattern arises in U is found for a given T. The probability being the number of occurrences of the pattern relative to the total number of subset S_q. The process is repeated for a number of values of T. In each case the probability P of the occurrences of all patterns is determined.

From the probability P the permutation entropy is defined as:

$$h(P) = -\sum_{i=1}^{M!} P_i \log P_i \tag{5.3}$$

The normalized PE is given as in ref. [25]:

$$H_P = h(P)/\log_2(M!) \tag{5.4}$$

Based on PE estimator values the amplitude of the valley is calculated as the valley signal to mean ratio (VSMR). The VSMR is denoted as H_V and defined in eq.(5.5).

$$H_v = \frac{x}{y} \tag{5.5}$$

Here $x = \left|(minH_P(\tau)_{|\tau \in V(\tau d)} - 1)\right|$ is the valley depth in the vicinity of τ_d and $y = \left|(< H_P(\tau) >_{|\tau \geq 0.5ns}) - 1\right|$ is the average depth value of harmonic and sub-harmonic valley.

5.3.1 Illustration of Permutation Entropy Calculation

Suppose U= (1,3,2,4,6,5,3,1,10,7) are chaotic output intensities of VCSEL in arbitrary unit and M = 3. Subsets S_q are formed as S_{q1} = (1,3,2), S_{q2} = (3,2,4), S_{q3} = (2,4,6), S_{q4} = (4,6,5), S_{q5} = (6,5,3), S_{q6} = (5,3,1), S_{q7} = (3,1,10) and S_{q8} = (1,10,7). Here T = 1. Subsets elements value pattern will be one of the element patterns as shown in table5.1. The obtained patterns of subset S_q are shown in table5.2. Table5.3 shows the occurrence and probability of the patterns.

Table 5.1

Patterns	Condition
PR1	$I_1 \geq I_2 \geq I_3$
PR2	$I_1 \geq I_3 \geq I_2$
PR3	$I_2 \geq I_1 \geq I_3$
PR4	$I_2 \geq I_3 \geq I_1$
PR5	$I_3 \geq I_2 \geq I_1$
PR6	$I_3 \geq I_1 \geq I_2$

Table 5.2

Subset	Elements	Pattern condition
S_{q1}	(1,3,2)	$I_2 \geq I_3 \geq I_1 \approx$ PR4
S_{q2}	(3,2,4)	$I_3 \geq I_1 \geq I_2 \approx$ PR6
S_{q3}	(2,4,6)	$I_3 \geq I_2 \geq I_1 \approx$ PR5
S_{q4}	(4,6,5)	$I_2 \geq I_3 \geq I_1 \approx$ PR4
S_{q5}	(6,5,3)	$I_1 \geq I_2 \geq I_3 \approx$ PR1
S_{q6}	(5,3,1)	$I_1 \geq I_2 \geq I_3 \approx$ PR1
S_{q7}	(3,1,10)	$I_3 \geq I_1 \geq I_2 \approx$ PR6
S_{q8}	(1,10,7)	$I_2 \geq I_3 \geq I_1 \approx$ PR4

Table 5.3

Patterns	Occurrence of pattern	Probability of pattern
PR1	2	2/8
PR2	0	0
PR3	0	0
PR4	3	3/8
PR5	1	1/8
PR6	2	2/8

The permutation entropy is calculated as

$$h(P) = -(\frac{2}{8}\log(\frac{2}{8}) + \frac{3}{8}\log(\frac{3}{8}) + \frac{1}{8}\log(\frac{1}{8}) + \frac{2}{8}\log(\frac{2}{8})) = 1.32$$

The normalized PE is calculated as

H_P = 1.32/log(6) = 0.7367

5.4 Experimental Results

The TD signature in the output intensity of chaotic VCSEL subject to variable polarization-angle of optical feedback is the focus of these investigations. First of all the polarization-resolved output intensities of the external cavity VCSEL are measured as a function of polarization angle θ_{PR}. The polarization of the VCSEL laser beam near threshold is linear and defined as the X-polarization (XP) direction; the Y-polarization (YP) is orthogonal to the X-polarization.

The power variation in the XP and the YP states as a function of polarization rotation θ_{PR} is shown in fig.5.3. The applied bias current is 6.5 mA and the feedback strength -14dB. In fig.5.3 the black line with circular symbols represents the XP state and the red line with star symbols represents the YP state of the VCSEL. It is seen that the YP state is the dominant lasing mode for polarization rotation angle θ_{PR} less than 50^o. When θ_{PR} increases beyond 50^o polarization switching occurs. For θ_{PR} greater than 80^o the XP mode becomes stable and dominant.

Section 5.4.2 explains the effects of fixed bias current of VCSEL and variable feedback sterngth on the TD concealment. The next section 4.3 explains the effect of variable bias current of VCSEL and fixed feedback sterngth on TD concealment.

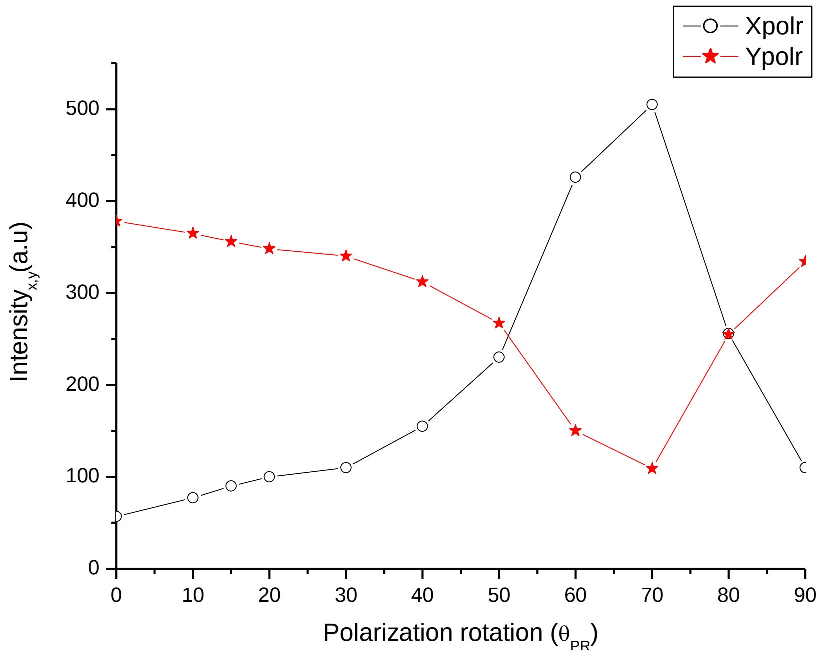

Fig.5.3 XP & YP resolved intensity of the VCSEL as a function of the polarization angle θ_{PR} at 6.5mA bias current and -14dB optical feedback strength. The black line with circular symbols represents the XP and the red line with star symbols represents the YP intensity.

5.4.1 Time Delay Identification

In this section the TD signature is studied using the auto-correlation function and the PE function. Peak at cavity round trip time is clearly visible in fig.5.4. Optical polarization-angle (θ_{PR} = 35^o) is considered here. Fig.5.4(a & b) shows the VCSEL output intensities in the time and frequency domains. The external cavity length in the experimental setup is 65cm so that the external cavity round trip time is 4.8ns. The relaxation oscillation period of the VCSEL used in the experiment was measured using Anritsu MS2667C (9KHz - 30GHz) spectrum analyzer. The observed relaxation oscillation period τ_{RO} of the VCSEL was 0.22ns. The auto correlation is calculated using eq.(5.1), with Δt values chosen from -10ns to 10ns in steps of 0.1ns. Fig.5.4(c) shows the auto correlation as a function of time delay. In fig.5.4(c) the highest peak is seen at a time delay of 4.8ns.This indicates that the TD of the external cavity has been retrieved. The PE is calculated using eq.(5.4), the sampling rate of data is 10GS/s and number of samples is 10^5. The PE as a function of the time delay is shown in fig5.4(d). Many valleys are seen in the figure due to the harmonics and sub-harmonics of the cavity time delay and τ_{RO}. In fig.5.4(d) the deepest valley is seen at TD 4.6 ns. This valley is close to the external cavity TD. Hence the cavity TD is also retrieved using the PE function.

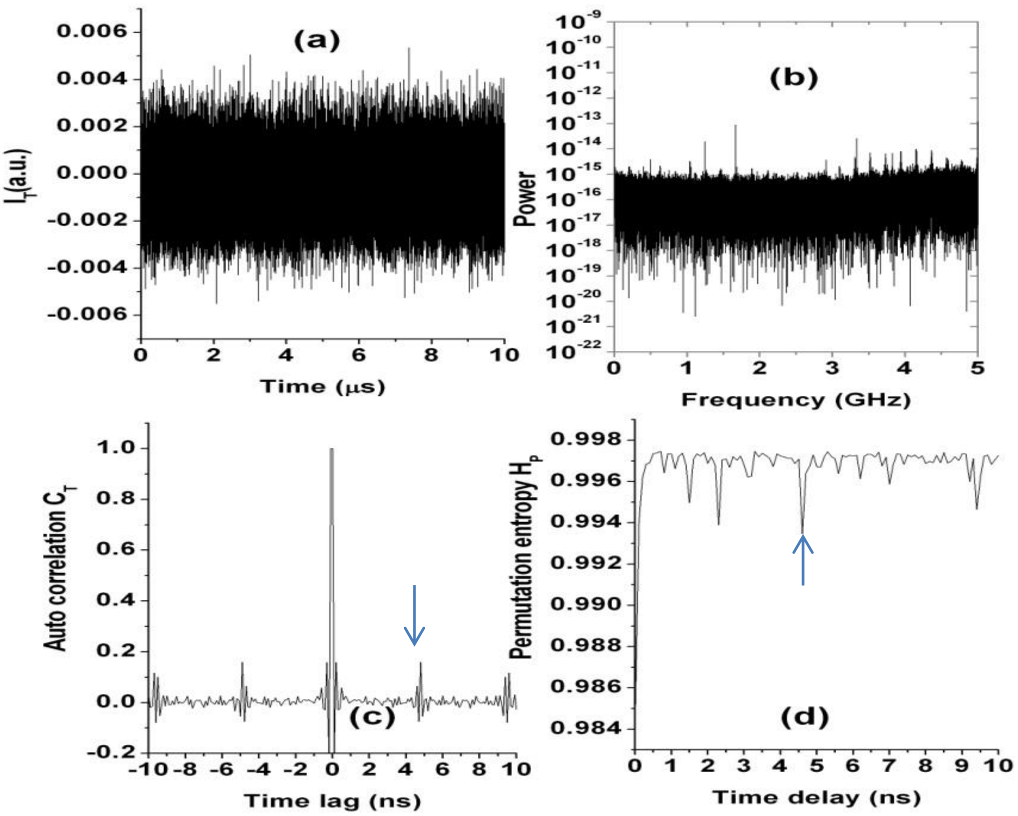

Fig.5.4.(a) VCSEL chaotic output intensity as function of time. (b) Frequency domain power spectrum of VCSEL output intensity. (c) Autocorrelation coefficient as function of time lag. (d) Permutation entropy as function of time delay at bias current 6.5mA, optical feedback strength -14dB and optical polarization-angle of feedback (θ_{PR}) is 35^o.

5.4.2 Effect of Polarization Varied Feedback on TD Concealment

It has been found theoretically that at low feedback strength the TD signature is concealed in the fully developed chaotic output of the VCSELs for all polarization-angles [22]. While for moderate feedback strength [22] found that the TD signature is concealed at intermediate polarization-angles. In this section the effect of feedback strength on time delay signature is studied experimentally.

The impact of the variation of the angle of polarization of the optical feedback on TD concealment is examined in fig.5.5. The results in fig.5.5 are obtained for an operating bias current of 6.5mA and feedback strength -14dB; the polarization angle θ_{PR} = 90^o. Fig.5.5(a& b) are plots of the chaotic output intensity of the VCSEL in the time domain and frequency domain respectively. It is seen in fig.5.5(c) that the auto-correlation function has no significant peak value, other than at Δt = 0ns. A similar characteristic of the PE function is observed in fig.5.5(d): there is no significant valley in the vicinity of the external cavity time delay. Thus the TD signature is completely masked in this case. On the other hand in fig.5.4 (which corresponds to the polarization angle θ_{PR}= 35^{o}, bias current 6.5mA and feedback strength -14dB) the TD signature peak is clearly seen in fig.5.4(c &d) in the vicinity of external cavity round trip time. Hence it is observed that the TD concealment is sensitive to the polarization-angle of optical feedback.

Next TD concealment is studied for different conditions of optical feedback strength and bias current of the VCSEL. The PSMR and VSMR are calculated using eq.(5.2) and eq.(5.5) respectively. It is observed from many autocorrelation function plots that: a visible peak close to τ_d always has C_P values greater than 6 and a peak close to τ_d and less prominent than a peak at τ_{RO} has C_P values less than 6. Hence a reference value C_{PR} = 6 is defined for the TD signature identification or concealment. i.e. if the value of C_P is greater than 6, the TD signature is considered as identified, otherwise the TD signature concealed.

Again in the case of PE estimation, it is observed from many PE function plots that a visible valley close to τ_d always has H_V values great than 2. While a valley close to τ_d and less prominent than a valley at τ_{RO} has H_V values less than 2. Hence a reference value H_{VR} = 2 is defined for the TD signature identification or the concealment. i.e. if the value of H_V is greater than 2, the TD signature considered as being identified, otherwise the TD signature is concealed.

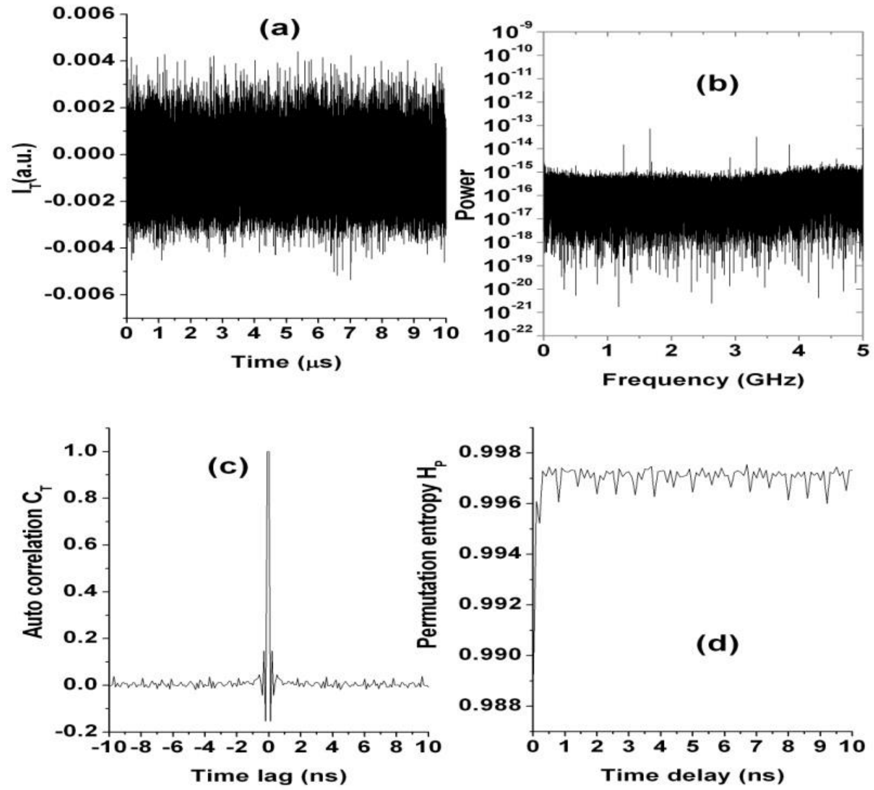

Fig.5.5 (a) VCSEL chaotic output intensity as function of time. (b) The power spectrum of the VCSEL output. (c) Auto-correlation function versus time lag and (d) PE function versus time delay at VCSEL bias current 6.5mA, feedback strength -14dB and optical polarization-angle of feedback (θ_{PR}) is 90^o.

The polarization states of the VCSEL are sensitive to the bias current. So it is important to explore the effect of feedback strength on TD concealment at different bias current of the VCSEL. In the next subsection the cases of bias currents 5.5mA, 6.0mA and 6.5mA are studied.

5.4.2.1 VCSEL Operating Bias Current 5.5mA

The PSMR and the VSMR as functions of the polarization angle for different feedback strengths are shown in fig.5.6. In fig.5.6 the operating bias current is 5.5mA. It is seen from fig.5.6(a) that the C_P values are smaller than C_{PR} for θ_{PR}> 75^o at the feedback strength = -18dB. Hence the TD is concealed for polarization angles θ_{PR}> 75^o. In the case of the fig.5.4(d) the H_V values are smaller than H_{VR} for θ_{PR}>20^o. It is observed in fig.5.6(b) that the C_P values are smaller than the C_{PR} for θ_{PR}> 80^o and in fig. 5.6(e) the H_V is smaller than the H_{VR} for θ_{PR}> 40^o at the feedback strength of -16dB. Hence the TD signature is concealed but the range of polarization angle for concealment is reduced. In fig.5.6(c & f) the feedback strength increases to -14dB. Fig.5.6(c) shows that the P_C values are always greater than P_{CR} While in fig.5.6(f) the H_V values are smaller than H_{VR} for $\theta_{PR} > 75^o$. Hence it is observed that the TD signature concealment is sensitive to the feedback strength. When the feedback strength increases there is reduction in polarization angle range (θ_{PR}) where TD concealment may be achieved.

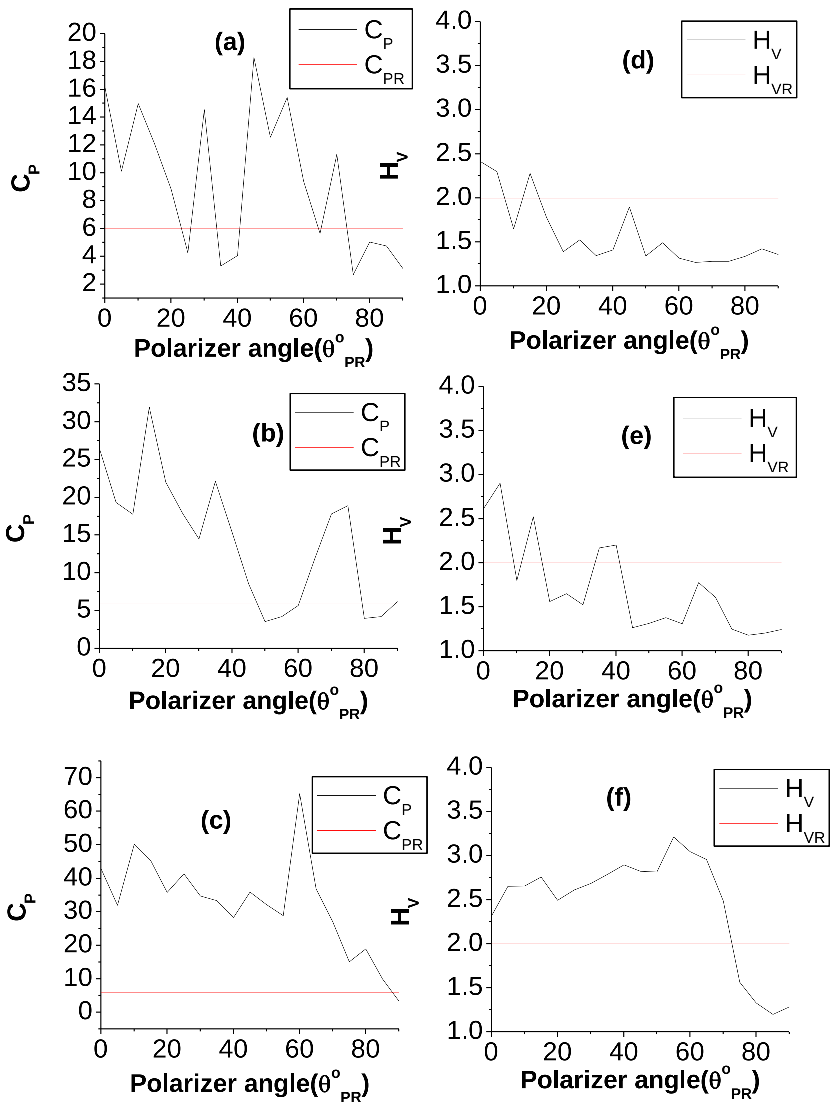

Fig.5.6(a, b& c) are PSMR as function of optical polarization-angle of feedback θ_{PR} at feedback strength -18dB, -16dB, -14dB respectively. (d, e, f) are the VSMR as function of polarization angle θ_{PR} at feedback strength -18dB, -16dB, -14dB respectively. The bias current is 5.5mA.

5.4.2.2 VCSEL Operating Bias Current 6.0mA

In this section the TD concealment is observed at VCSEL operating bias current 6.0mA and feedback strengths of -18dB, -16dB and -14dB. It is seen from fig.5.7(a) that the C_P values are smaller than C_{PR} for $\theta_{PR}> 45^o$ at the feedback strength = -18dB. Hence the TD is concealed for polarization angles $\theta_{PR}> 45^o$. In the case of the fig.5.7(d) the H_V values are smaller than H_{VR} for all polarization angles θ_{PR}. Thus the PE function shows that the TD signature is concealed. It is observed in fig.5.7(b) that the C_P values are close to the C_{PR} for $\theta_{PR}> 35^o$ and in fig.5.7(e) the H_V is smaller than the H_{VR} for $\theta_{PR}> 20^o$ at the feedback strength of -16dB. Hence the TD signature is concealed but the range of polarization angles for concealment is reduced. In fig.5.7(c & f) the feedback strength increases to -14dB. Fig.5.7(c) shows that the P_C values are smaller than P_{CR} for $\theta_{PR}>$ 70^o, while in fig.5.7(f) the H_V values are smaller than H_{VR} for $\theta_{PR}> 65^o$. Hence the feedback strength increases the TD concealment angle of polarization range (θ_{PR}) reduces. Thus it is observed that the TD signature concealment is sensitive to the polarization angle θ_{PR}.

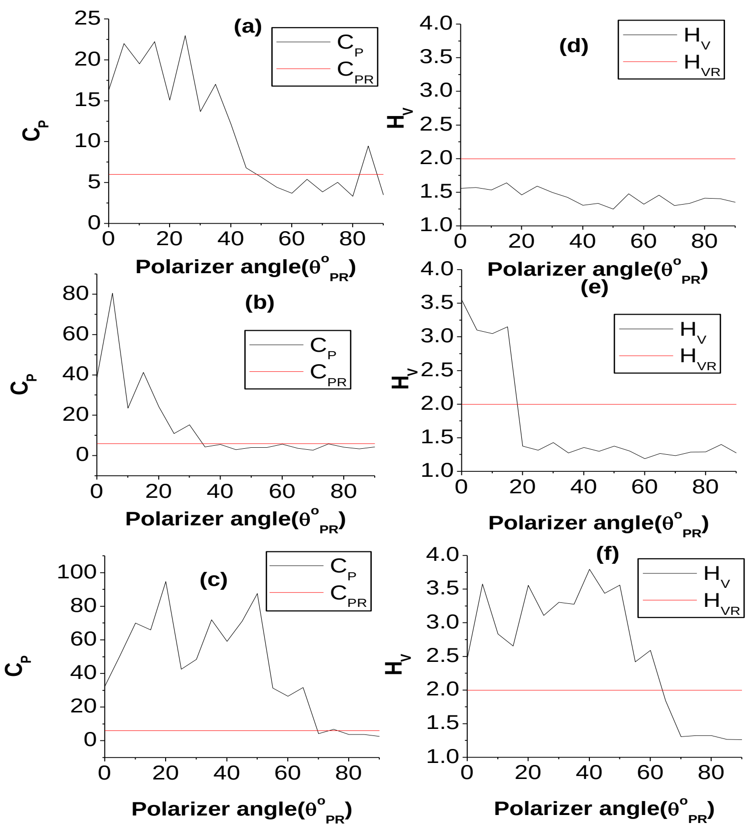

Fig.5.7(a, b& c) are PSMR as function of optical polarization-angle of feedback θ_{PR} at feedback strength -18dB, -16dB, -14dB respectively. (d, e, f) are the VSMR as function of polarization angle θ_{PR} at feedback strength -18dB, -16dB, -14dB respectively. The bias current is 6.0mA.

5.4.2.3 VCSEL Operating Bias Current 6.5mA

In this section TD concealment is studied at a VCSEL bias current 6.5mA. The PSMR and the VSMR as functions of the polarization angle for different feedback strengths are shown in fig.5.8. It is seen from fig.5.8(a) that the C_P values are smaller than C_{PR} for θ_{PR}> 35^o for a feedback strength of -18dB. Thus the TD is concealed for polarization angles θ_{PR}> 35^o. In the case of fig.5.8(d) the H_V values are smaller than H_{VR} for all polarization angles θ_{PR}. Thus the PE function shows that the TD signature is concealed. It is observed in fig.5.8(b) that the C_P values are smaller than the C_{PR} for θ_{PR}> 45^o and in fig.5.8(e) the H_V is smaller than the H_{VR} for θ_{PR}> 20^o at the feedback strength of -16dB. In this case the TD signature is concealed but the range of polarization angle of concealment is reduced. Fig.5.8(c) shows that the P_C values are smaller than P_{CR} for θ_{PR}> 60^o and in fig.5.7(f) the H_V values are smaller than H_{VR} for θ_{PR}> 45^o. Hence it is observed from the previous sections that while increasing the VCSEL operating bias current the TD concealment is sensitive to the polarization angle of optical feedback and feedback strength. So the TD concealment can be achieved for the flexible operational bias current range. From fig.5.3 it is seen that the polarization angle near 50^o, the XP intensity values and the YP intensity values are close to each other. So the interaction between the XP and the YP feedback light becomes stronger. Hence strong interaction leads to the better concealment of the TD signature.

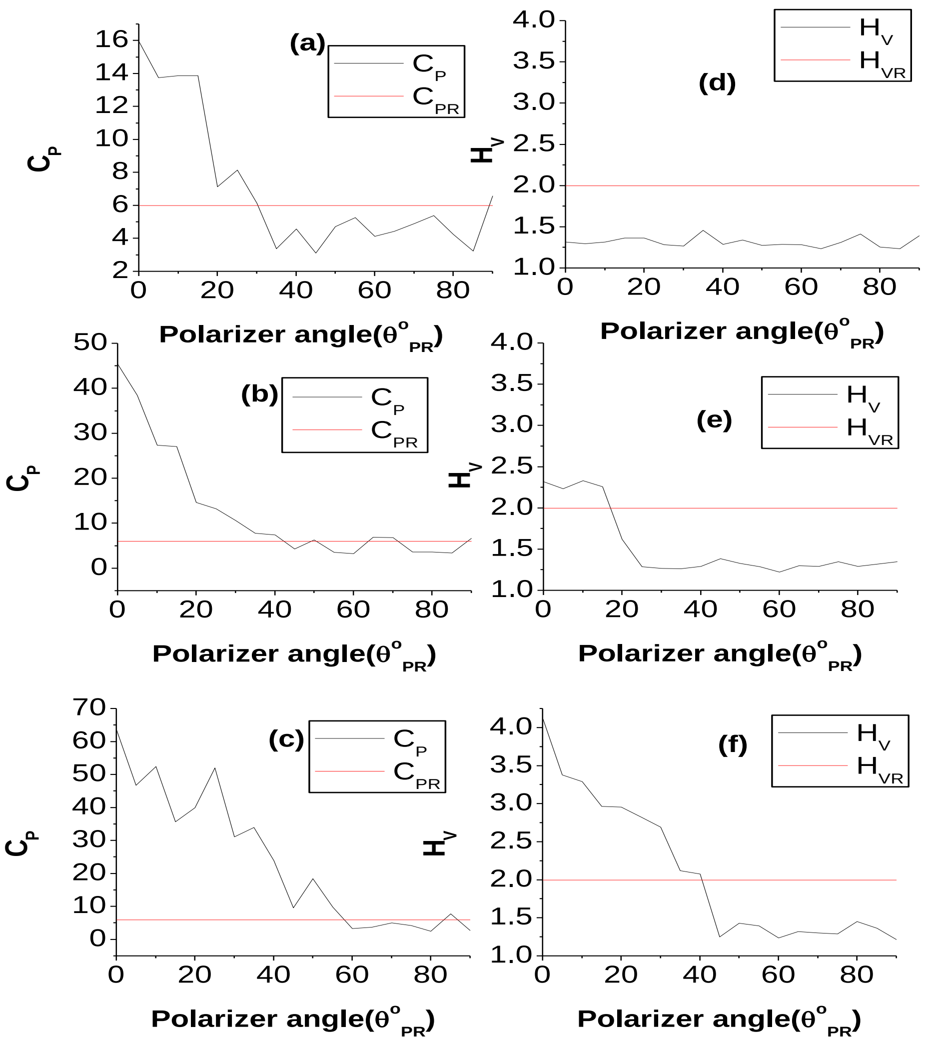

Fig.5.8(a, b& c) are PSMR as function of optical polarization-angle of feedback θ_{PR} at feedback strength -18dB, -16dB, -14dB respectively. (d, e, f) are the VSMR as function of polarization angle θ_{PR} at feedback strength -18dB, -16dB, -14dB respectively. The bias current is 6.5mA.

To elucidate the effect of both feedback strength and the polarization angle θ_{PR} on TD concealment, a convenient approach is to utilise contour plots of PSMR and VSMR as a function of feedback strength and polarization angle θ_{PR}. The contour plot will be helpful for finding optimal operating parameters for the TD concealment region. Fig.5.9 is a contour plot of PSMR and VSMR as function of feedback strength and polarization angle θ_{PR} at a bias current 6.5mA. The red regions are the lowest values of C_P and H_V; so red area represents the TD concealed region. It is observed from fig.5.9(a&b) that the TD signature is concealed for polarizer angles $\theta_{PR}>30^o$ and lower feedback strengths.

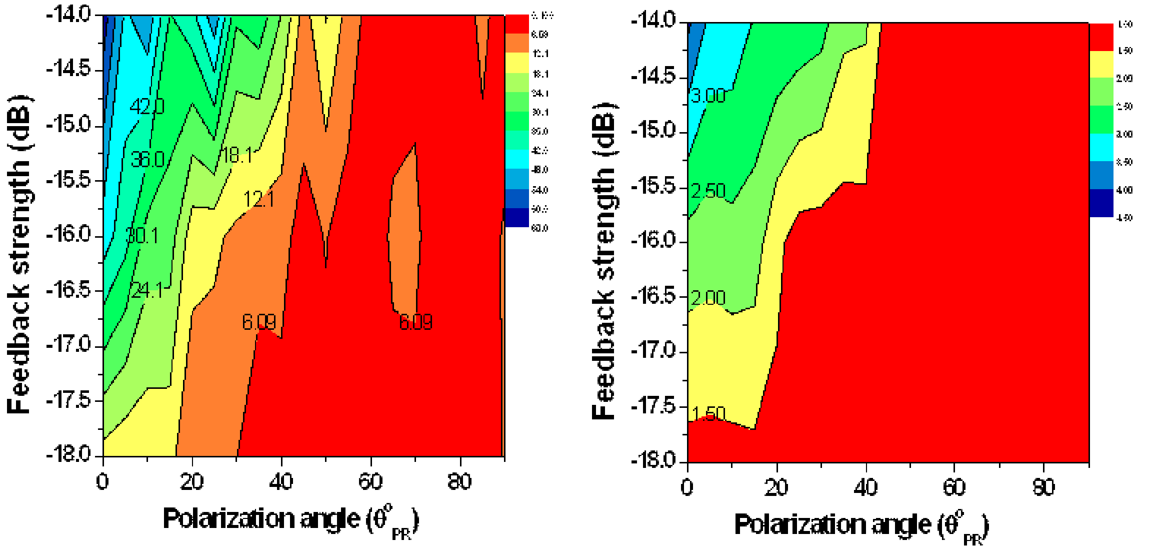

Fig.5.9(a) PSMR contour as a function of the feedback strength and the optical polarization-angle of feedback at bias current 6.5mA.

Fig.5.9 (b) VSMR contour as a function of the feedback strength and the optical polarization-angle θ_{PR} of feedback at bias current 6.5mA.

5.4.3 Effect of Varied Bias Current of VCSEL on TD Concealment

In section 4.2 the effects of varying optical feedback strength at fixed bias current on TD concealment were explained. In the present section outcomes of measuring the influence of varying bias current at fixed feedback strength on TD concealment are discussed. The optical feedback strength used in this case is fixed at -14dB. The measurement is performed at bias currents of 5.5mA, 6.0mA and 6.5mA. In fig. 5.10(a) the bias current is 5.5mA. Here it is seen that the values of C_P are greater than C_{PR} for all polarization angles θ_{PR}, however in fig. 5. 10(d) the PE function measurements show that the H_V is greater than H_{VR} for polarization angles $\theta_{PR}< 80^o$. As such TD signature concealment is observed for a narrow range of polarizer angles. In fig. 5. 10(b) the bias current is 6mA, TD signature concealment is observed for polarization angles θ_{PR}> 70^o, the same TD concealment is seen in fig. 5.10(e) using the PE function. The effect of further increased bias current to 6.5mA is shown in fig. 5.10(c). There it is apparent that TD signature concealment occurs near the polarization angle θ_{PR}> 60^o from the autocorrelation function measurement whereas the PE function measure is shown in fig. 5.10(f). In fig. 5.10(f) the TD signature concealment occurs for polarization angles θ_{PR}> 40^o. Hence the TD signature concealment with varying polarization angles of optical feedback is sensitive to the bias current of the VCSEL. The theoretical prediction in ref. [22] indicates that at higher bias currents wider regions of TD concealment polarization angle at moderate feedback strength can be obtained. Experimentally it is seen in fig. 5.10 that higher bias current improves the TD signature concealment.

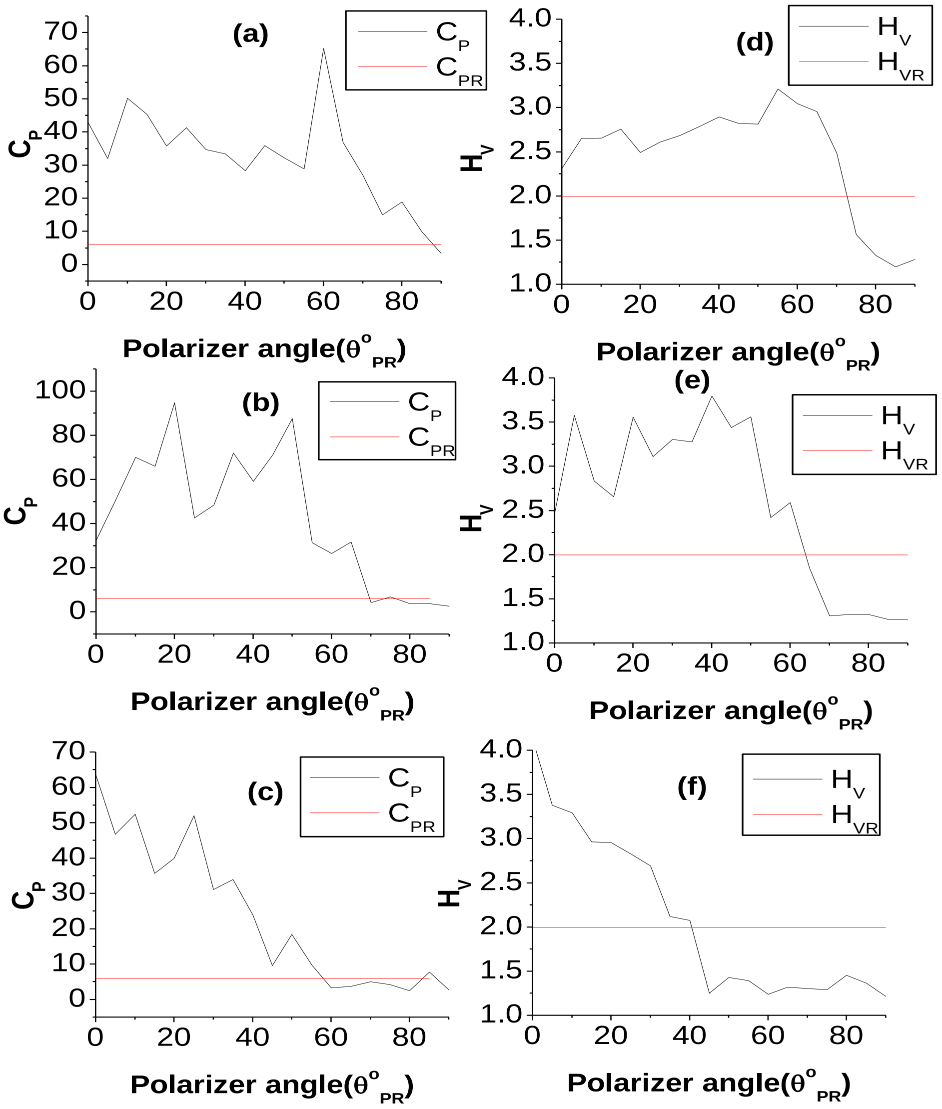

Fig.5.10(a, b & c) PSMR as the function of optical polarization-angle of feedback θ_{PR} at bias current 5.5mA, 6.0mA and 6.5mA respectively. (d, e, f) are the VSMR as function of optical polarization-angle of feedback θ_{PR} at bias current 5.5mA, 6.0mA and 6.5mA respectively. The feedback strength is -14dB.

5.5 Conclusion

A system with external optical feedback incorporates periodic temporal components related to the time delay (TD) associated with the external cavity formed between the laser and the external mirror. Such time delay signatures may be regarded as an additional key to encode messages in optical chaos communication. It is important that no eavesdropper can determine the time delay. For this reason time delay signature concealment for external cavity semiconductor lasers subject to variable optical polarization-angle of the feedback has been studied experimentally. The experimental work has focused on the influence of the optical polarization-angle of feedback, feedback strength and the VCSEL bias current. TD signature concealment is observed for lower feedback strength and intermediate polarizer angles. The effect of bias current on time delay concealment has been determined. At lower bias currents TD signature concealment occurs over narrow polarizer angle ranges ($70^o<\theta_{PR}<90^o$), whilst for larger bias currents wider polarizer angle ranges ($45^o<\theta_{PR}<90^o$) allow TD signature concealment. The observed results are consistent with previous theoretical predictions [22]. The operational parameter values for TD concealment in the external cavity VCSEL system will provide significant information for designing secure optical chaos communication systems.

References

[1] A. Argyris, D. Syvridis, L. Larger, V. Annovazzi-Lodi, P. Colet, I. Fischer, J. García-Ojalvo, C. R. Mirasso, L. Pesquera, and K. A. Shore,"Chaos-based communications at high bit rates using commercial fibreoptic links," Nature, vol. 438, pp. 343–346, Nov. 2005.

[2] K. E. Chlouverakis and M. J. Adams, "Optoelectronic realisation of NOR logic gate using chaotic two-section lasers," IEE Electronics Letters, vol.41, pp. 359–360, Mar. 2005.

[3] A. Uchida, K. Amano, M. Inoue, K. Hirano, S. Naito, H. Someya, I. Oowada , T. Kurashige, M. Shiki, S. Yoshimori, K. Yoshimura, and P. Davis, "Fast physical random bit generation with chaotic semiconductor lasers," Nature Photon., vol. 2, pp. 728–732,Nov. 2008.

[4] I. Kanter, Y. Aviad, I. Reidler, E. Cohen, and M. Rosenbluh, "An optical ultrafast random bit generator," Nature Photon., vol. 4, pp. 58–61, Dec. 2010.

[5] M. J. Bünner, M. Popp, T. Meyer, A. Kittel, and J. Parisi, "Tool to recover scalar time-delay systems from experimental time series," Phys. Rev. E, vol. 54, pp. 3082–3085, Jul. 1996.

[6] R. Hegger, M. J. Bünner, and H. Kantz, "Identifying and modelling delay feedback systems,"Phys. Rev. Lett., vol. 81, pp. 558–561, Jul. 1998.

[7] D. Rontani, A. Locquet, M. Sciamanna, and D. S. Citrin, "Loss of time-delay signature in the chaotic output of a semiconductor laser with optical feedback," Opt. Lett., vol. 32, pp. 2960–2962, 2007.

[8] D. Rontani, A. Locquet, M. Sciamanna, D. S. Citrin, and S. Ortin, "Time-delay identification in a chaotic semiconductor laser with optical feedback: a dynamical point of view," *IEEE J.* Quantum Electron., vol. 45, pp. 879–891, 2009.

[9] R.Vicente, J. Dauden, P. Colet, and R. Toral, "Analysis and characterization of the hyperchaos generated by a semiconductor laser subject to a delayed feedback loop," IEEE J. Quantum Electron., vol. 41, pp. 541–548, Apr. 2005.

[10] M. J. Bünner, M. Popp, T. Meyer, A. Kittel, and J. Parisi, "Tool to recover scalar time-delay systems from experimental time series," Phys. Rev. E Stat. Phys. Plasmas Fluids Relat. Interdiscip. Topics, vol. 54, no. 4, pp. R3082–R3085, 1996.

[11] H. Voss and J. Kurths, "Reconstruction of nonlinear time-delayed feedback models from optical data," Chaos Solitons Fractals, vol. 10, no. 4, pp. 805–809, 1999.

[12] S. Ortin, J. M. Gutierrez, L. Pesquera, and H. Vasquez, "Nonlinear dynamics extraction for time-delay systems using modular neural networks synchronization and prediction," Phys. A, vol. 351, no. 133, pp. 133–141, 2005.

[13] V. S. Udaltsov, L. Larger, J. P. Goedgebuer, A. Locquet, and D. S. Citrin, "Time delay identification in chaotic cryptosystems ruled by delay-differential equations," J. Opt. Technol., vol. 72, no. 5, pp. 373–377, 2005.

[14] R. Hegger, M. J. Bünner, H. Kantz, and A. Giaquinta, "Identifying and modeling delay feedback systems," Phys. Rev. Lett., vol. 81, no. 3, pp. 558–561, 1998.

[15] M. D. Prokhorov, V. I. Ponomarenko, A. S. Karavaev, and B. P. Bezruchko, "Reconstruction of time-delayed feedback systems from time series," Phys. D, Nonlinear Phenomena, vol. 203, nos. 3–4, pp. 209–223, 2005.

[16] N. Li, W. Pan, S. Xiang, L. Yan, B. Luo, X. Zou, L. Zhang and P. Mu, "Photonic Generation of Wideband Time-Delay-Signature-Eliminated Chaotic Signals Utilizing an Optically Injected Semiconductor Laser," IEEE J. Quantum Electron., vol. 48, pp. 1339–1345, 2012.

[17] J. Wu, Z. Wu, X. Tang, X. Lin, T. Deng, G. Xia and G. Feng, "Simultaneous Generation of Two Sets of Time Delay Signature Eliminated Chaotic Signals by

Using Mutually Coupled Semiconductor Lasers," IEEE Phot. Technol. Lett., vol. 23, pp. 759-761, 2011

[18] A. Scire, J. Mulet, C.R. Mirasso, J. Danckaert, M.S. Miguel, "Polarization Message Encoding through Vectorial Chaos Synchronization in Vertical-Cavity Surface-Emitting Lasers," Phys. Rev. Lett., vol. 90, 113901, 2003.

[19] M. Sciamanna, I. Gatare, A. Locquet, K. Panajotov, "Polarization synchronization in unidirectionally coupled vertical-cavity surface-emitting lasers with orthogonal optical injection," Phys. Rev. E, vol. 75, 056213, 2007.

[20] Y. Hong, M.W. Lee, J. Paul, P.S. Spencer, K.A. Shore, "GHz Bandwidth Message Transmission Using Chaotic Vertical-Cavity Surface-Emitting Lasers," IEEE J. Lightw.Technol., vol. 27, pp. 5099, 2009.

[21] Y. Hong, P. S. Spencer and K. A. Shore, "Enhancement of Chaotic Signal Bandwidth in Vertical-Cavity Surface-Emitting Lasers with Optical Injection," J. Opt. Soc. Am. B, vol.29, pp. 415-419, 2012.

[22] S. Xiang , W. Pan, B. Luo, L. Yan, X. Zou, N. Jiang, L. Yang, H. Zhu, "Conceal time-delay signature of chaotic vertical-cavity surface-emitting lasers by variable-polarization optical feedback," Optics Communications, vol. 284, pp. 5758-5765, 2011.

[23] M. W. Lee, P. Rees, K. A. Shore, S. Ortin, L. Pesquera, and A. Valle, "Dynamical characterisation of laser diode subject to double optical feedback for chaotic optical communications," *IEE Proc*. Optoelectron., vol. 152, pp. 97–102, Apr. 2005.

[24] C. Bandt and B. Pompe, "Permutation entropy: a natural complexity measure for time series," *Phys. Rev. Lett.*, vol. 88, 174102, 2002.

[25] M. C. Soriano, L. Zunino, O. A. Rosso, I. Fischer, C. R. Mirasso, "Time Scales of a Chaotic Semiconductor Laser With Optical Feedback Under the Lens of a Permutation Information Analysis," IEEE J. Quantum Electron., vol. 47,pp. 252, 2011.

Chapter 6
Summary and Future Work

6.1 Summary

This thesis has examined theoretically and experimentally aspects of the use of external cavity semiconductor lasers for secure optical communications.

Theoretical work has identified an optimal operating condition where high-quality chaos synchronization coincides with maximum message extraction efficiency.

With a view to practical deployment of laser-diode based optical chaos communications, attention has been focused on using the receiver laser bias current as an experimentally adjustable physical quantity to achieve the defined ideal operating conditions. Use of such an operating regime will facilitate practical deployment of optical chaos communications systems without the need for re-adjustment of laser operating conditions in the field.

Numerical simulations are performed on analogue and digital message modulation using the Lang-Kobayashi model of external cavity semiconductor lasers. The cross-correlation function is used to measure the synchronization between the TL and RL. Message recovery efficiency is calculated using SNR and BER for analogue and digital message modulation respectively.

An optimal operating condition is identified where high-quality chaos synchronization coincides with maximum message extraction efficiency. With a view to practical deployment of laser-diode based optical chaos communications, attention has been focused on using the receiver laser bias current as an experimentally adjustable physical quantity to achieve the defined ideal operating conditions. In this way it has been found that an optimal configuration for 1GHz modulation frequency may utilize a 2% modulation depth and 20% TL-RL coupling rate. Having established a methodology for identifying the defined optimal operating conditions approach more generally. Specific interest applied to digital message transmission with a view to identifying optimal Bit-Error-Rates (BER). In that context the modulation frequency dependences of the performance will have particular relevance.

Optimal operating conditions have been identified for a digital optical chaos communication system. Different conditions of message transmission rate, modulation depth and coupling rate have been examined. In this way it has been found,for example, that an optimal configuration for 2GB/s message transmission may utilize a 1.8% modulation depth and 20% TL-RL coupling rate.

In chapter 5, time delay signature concealment of chaotic vertical cavity semiconductor lasers with variable optical polarization-angle of feedback has been studied experimentally. Auto-correlation function-based peak signal to mean ratio and permutation entropy function based valley signal to mean ratio methods were used to determine the time delay concealment. The experimental work has focused on the influence of the optical polarization-angle of feedback, feedback strength and the VCSEL bias current. TD signature concealment is observed for lower feedback strength and intermediate polarizer angles. The effect of bias current on time delay concealment has been determined. At lower bias currents TD signature concealment occurs over narrow polarizer angle ranges ($70^o<\theta_{PR}<90^o$), whilst for larger bias currents wider polarizer angle ranges ($45^o<\theta_{PR}<90^o$) allow TD signature concealment. The observed results are consistent with previous theoretical predictions [22]. The operational parameter values for TD concealment in external cavity VCSEL system will provide significant information for designing secure optical chaos communication systems.

6.2 Future work

This thesis opens two interesting lines of research for future work. The central interest is chaos generation using semiconductor lasers.

One further line of research can be focused on the physical generation of random numbers using chaotic semiconductor lasers.

The techniques of random number generation can be classified into two categories: pseudorandom number generators and physical random number generators. Pseudorandom numbers are generated from a single random seed using deterministic algorithms. However, sequences of pseudorandom numbers generated deterministically from the same seed will be identical, and this can cause serious problems for applications in security.

For this reason, chaos can be used as a nondeterministic random number generator. A suitable source of nondeterministic random number generation can be chaotic semiconductor lasers. A physical optical random number generator can be proposed using an external cavity VCSEL with variable optical-polarization-angle feedback. In this way, random numbers can be generated at rates greater than tens of gigabit per second.

Another development of the research could feature chaotic optical logic gates. Chaotic systems show sensitivity to initial conditions and yields diverging outcomes, i.e. the chaotic system can be implemented to generate many different patterns with a single hardware. A chaotic semiconductor laser may be used to implement such chaotic logic. For example, a transmitter-receiver coupled lasers system can be proposed for chaotic optical logic gate operation. The polarization of the receiver laser switches between two linear orthogonal polarizations (referred to as X and Y) in response to changes in the injection strength of the transmitter laser. Different injection levels can enable codifying the input combination of OR or AND logic gates. The output light polarizations of the receiver laser can give the logic response e.g. 1 for X-polarized light and 0 for Y-polarized light.